EXPERIMENTAL INVESTIGATIONS OF MUONIC X-RAY TRANSITIONS IN MERCURY ISOTOPES

Thesis by
Alan Andrew Hahn

In Partial Fulfillment for the Requirements

for the degree of

Doctor of Philosophy

California Institute of Technology
Pasadena, California

1978

(Submitted October, 1977)

Acknowledgments

I would like to thank my advisor, Dr. Felix Boehm, for his many years of support and encouragement during my graduate career at Caltech. The advice and asisstance of Dr. Richard J. Powers in both the experiment and data analysis are gratefully acknowledged. I would also like to achnowledge the many enlightening discussions with Dr. Petr Vogel and Dr. Jean-Luc Vuilleumier. The assistance of Herb Henrikson and Patrick McCrea in the construction of the target frame and scintillators was invaluable. The cooperation of Dr. Robert Siegel and his staff at the Space Radiation Effects Laboratory is appreciated. I would also like to acknowledge the assistance of Teresa Warren in the off-line analysis of the 100 list tapes during my stay in Newport News, Virginia.

I would like to thank the U.S. ERDA, California Institute of Technology, and my wife for generous financial support during my five years as a graduate student.

I express my graditude to my sister-in-law and typist, Patricia Hofmann, who cheerfully (at times) put up with the many revisions of this thesis.

In conclusion, I would like to thank my wife Eileen for her moral support during the years of graduate work. Her artistic effort is also acknowledged for Figure 3 of this thesis.

ABSTRACT

Muonic x-ray spectra have been measured for six Hg isotopes with mass numbers 198, 199, 200, 201, 202, and 204. From the measurements we have determined the half-density radii c of the monopole charge distributions assuming a Fermi-like function. In the even isotopes we have extracted the spectroscopic quadrupole moments (Q_s) of the 2+ nuclear states. In ^{199}Hg we have determined $Q_s(I)$ and $B(E2;1/2^- \rightarrow I^-)$ for the 158 keV (I=5/2) and 208 keV (I=3/2) nuclear states. In ^{201}Hg the ground state spectroscopic moment $Q_s(3/2^-)$ was obtained. The analysis of the other E2 moments in ^{201}Hg is contingent on the improved knowledge of the nuclear level structure. Isotope shifts have been determined and analyzed in terms of δR_k and are compared to e^- x-ray and optical IS measurements. We present evidence of the E1 excitation of a 5.65 MeV 1^- nuclear state in ^{202}Hg.

TABLE OF CONTENTS

TABLE OF CONTENTS (continued)

LIST OF FIGURES

SECTION 1.0
INTRODUCTION

Within the last ten years there has been a growing theoretical and experimental interest in the nuclear structure of the Hg isotopes. In light of this it is surprising that relatively little information has existed on the nuclear charge distribution of the stable isotopes, (196, 198, 199, 200, 201, 202, and 204). This has been due in part to the unavailability of sufficient quantities of enriched isotopes. This still remains the case for ^{196}Hg. The literature contains no work based on electron scattering. The only previous experiment designed to study charge distributions in Hg was a muonic x-ray study[1] using natural Hg as a target. Unfortunately, most of the stable isotopes occur in appreciable amounts in natural Hg. As a result, one cannot unfold the data to recover information from any single isotope.

In this thesis we present results of measurements of muonic x-rays in separated isotope samples of Hg with the mass numbers 198, 199, 200, 201, 202, and 204. From our data we were able to determine the radius of the monopole charge distribution. In addition we present accurate values for the isotope shifts of several muonic charge radii between neighboring isotopes. Furthermore, we have investigated the static and dynamic quadrupole interaction in several Hg isotopes. Electric quadrupole moments are presented, preceded by a discussion of the nuclear excitation mechanisms.

Early theoretical calculations[2] have assumed that the even Hg isotopes were spherical since they are but two protons removed from the doubly magic spherical nucleus ^{208}Pb. However, more recent calculations[3,4,5] abandon this assumption and predict an oblate shape and a positive sign for the spectroscopic quadrupole moment of the 2+ state ($Q_s(2+)$). Two recent experiments utilize the reorientation effect in Coulomb excitation to measure $Q_s(2+)$. Esat et al.[6] determined a $Q_s(2+)$ in ^{198}Hg which is consistent in both sign and magnitude with theory. Bockisch et al.[7] on the other hand, have found a negative sign for $Q_s(2+)$. Our data favor the positive $Q_s(2+)$ for all even isotopes in agreement with Esat et al. and theory.

Theoretical calculations for the odd isotopes $^{199,201}Hg$ are indeed sparse. Variations of De Shalit's weak coupling model[8] have been made for ^{199}Hg[9,10]. Only the later reference predicts values for $Q_s(5/2^-, 158\ keV)$ and $Q_s(3/2^-, 208\ keV)$ and they are not in accordance with our findings. Experimental data from lifetime[11] and Coulomb excitation[11] measurements have determined the E2 excitation probabilities, $B(E2; 1/2^- \rightarrow 5/2^-; 158\ keV)$ and $B(E2; 1/2^- \rightarrow 3/2^-; 208\ keV)$. We have independently determined these quantities and they are in reasonable agreement with the above. The theoretical interpretation of the ^{201}Hg spectra remains somewhat of an enigma. There is no nuclear model which describes the observed level structure[12]. Kalish et al.[11] could find no evidence of any Coulomb excitation in ^{201}Hg. While we do find some E2 excitation our analysis indicates the need of a low lying ($\sim$ 30 keV) $5/2^-$ level which has not yet been positively established from other experiments.

The shift in energy of muonic x-rays (or any other atomic transition) between two isotopes, referred to as isotope shift, is a powerful tool to investigate the variation of the nuclear charge distribution as neutrons are added to the nucleus. By 1964 optical spectroscopists using conventional spectroscopic techniques, had already established Hg as being the most complete study of isotope shift in any isotope chain. The range of their measurements extended from ^{192}Hg to ^{204}Hg with some isotopes having radioactive half-lives as short as one hour. Now sophisticated online separation and optical pumping techniques have extended the range to twenty isotopes, from ^{181}Hg to ^{205}Hg with half-lives as short as 3.6 seconds. In 1971 Bonn et al.[13] discovered an abrupt discontinuity of the isotope shift between ^{187}Hg and ^{185}Hg. Referring to Figure 1, the optical isotope shift (in GHz) shows a remarkably constant slope starting from ^{204}Hg down to ^{187}Hg. The currently accepted explanation for this abrupt discontinuity is that the intrinsic nuclear shape suddenly changes from slightly oblate to strongly prolate. This large change in nuclear deformation has an effect upon the RMS nuclear radius of the monopole charge density (to which the optical shifts are sensitive).

Attempts to compare the optical isotope shifts to the calculated shifts $\delta\langle r^2\rangle$ of the nucleus meet with difficulties since the experiment measures the product of $\delta\langle r^2\rangle$ and an atomic factor relating the electron density at the nucleus of a particular electronic configuration. Hartree-Fock atomic calculations are used to determine the atomic factor. At present these calculations have an estimated uncertainty

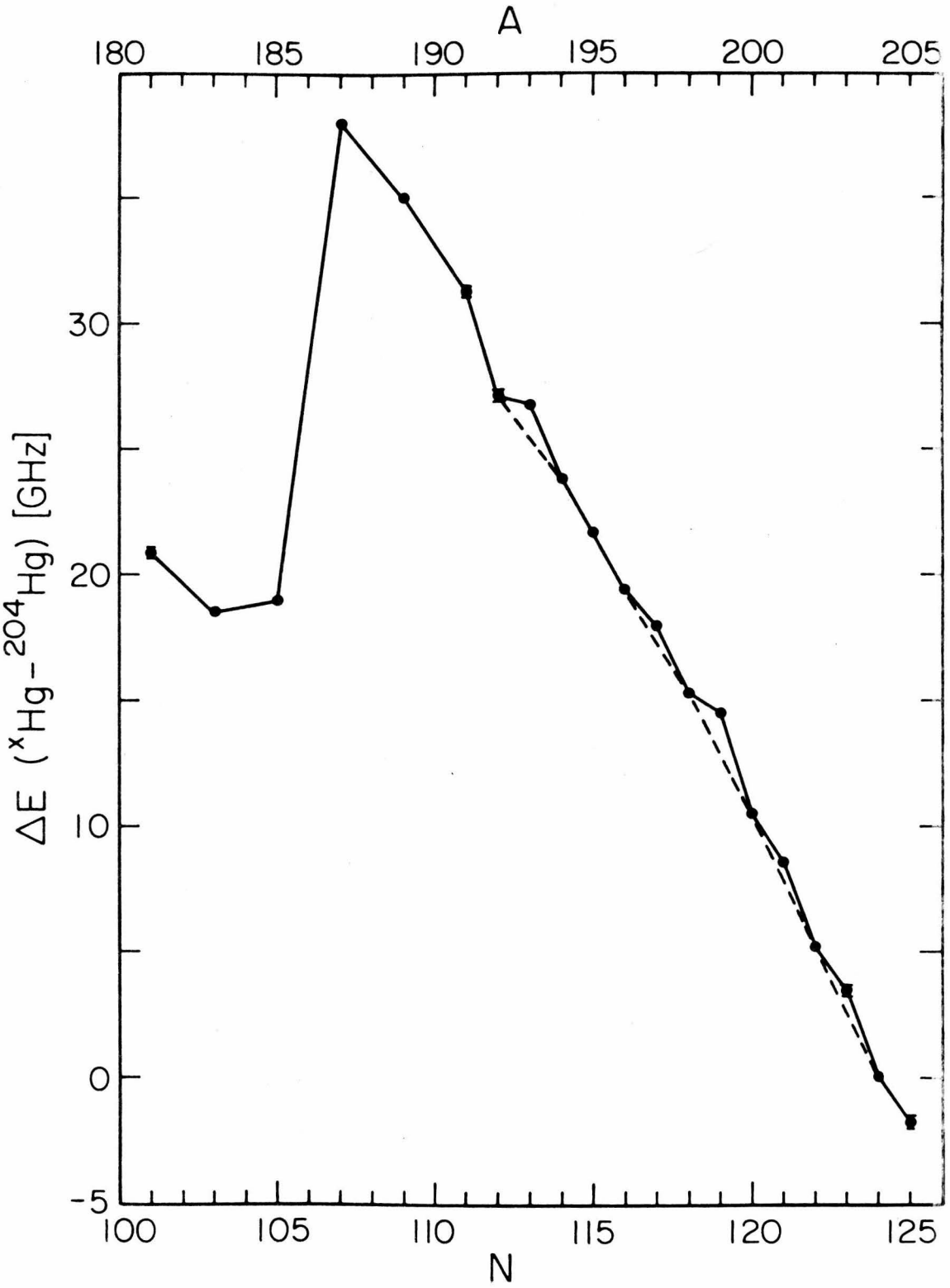

FIGURE 1

Hg isotope shifts as measured by optical transitions[49]. Both solid and dashed lines are drawn to guide the eye. The even-odd staggering of the isotopes is evident.

of 10-30% (which is common to all isotopes in Hg).[14] Traditionally one uses $\delta\langle r^2\rangle$ determined by electronic K x-ray isotope shifts to normalize the optical shifts since the theoretical calculations in this case are accurate to 1% or better. However, the experimental values in Hg[15] are themselves at best only 10% accurate. Our muonic x-ray isotope shifts may be used for the renormalization of the optical shifts since our combined theoretical and experimental uncertainties in the even isotopes have an error of only 3%. Thus the optical isotope shifts may all be converted by our results into absolute nuclear $\delta\langle r^2\rangle$ units.

The present thesis is divided into six sections. In section two the atomic theory of the muonic atom is briefly described, stressing the E2 hyperfine interaction. Section three is concerned with our experimental setup. The data analysis is described in section four with emphasis upon our model dependent assumptions. The results for each isotope are presented in section five. A detailed description is given here of the parameterization of the isotope shift in terms of the generalized radial moment analysis and comparisons are made with the optical and e^- K x-ray shifts. An outlook for future experimental and theoretical work is given in section six.

SECTION 2.0
ATOMIC THEORY

In this section we present a brief review of the theoretical basis of muonic atoms and muonic x-ray emission. Detailed discussions on the theory of muonic atoms can be found in reference[16].

2.1 Atomic Level Structure

The muon-nucleus Hamiltonian may be formally written as follows,

$$H = H_\mu + H_N + H' + H_{int} , \tag{2.1}$$

where H_μ is the Dirac Hamiltonian for a muon in a spherically symmetric electric potential composed of the nuclear Coulomb field and the first order vacuum polarization. H_N is the nuclear Hamiltonian in the absence of the muon, and H' denotes contributions from additional radiative corrections, nuclear polarization and other corrections listed below. H_{int} describes the higher order interactions between the muon and the nuclear multipole field, primarily arising from the M1 and E2 moments.

It is convenient to parameterize the solutions to H_μ by assuming an axially symmetric nuclear charge distribution of the form

$$\rho_N(r,\theta) = \rho_o(r) + \rho_{20}(r)\, Y_{20}(\theta) + \cdots , \tag{2.2}$$

with

$$\rho_o(r) = \rho_N\{1 + \exp[4\ln 3(r-c)/t]\}^{-1}. \qquad (2.3)$$

The unperturbed muonic eigenfunctions and eigenvalues of H_μ are calculated with the "Fermi function-like" distribution $\rho_o(r)$. The parameters c and t are the half-density radius and the 90-10% skin thickness, respectively. The generation of $\rho_{20}(r)$ is ignored in the present section but will be taken up in Section 4.4 on model dependence. The modified computer code of McKee is used to numerically integrate the eigenvalue equation and to solve for the eigenfunctions and energy eigenvalues.

The corrections from H' to the muon energy are:

1. Higher order vacuum polarization corrections of Blomqvist[17] of up to the order $\alpha(Z\alpha)^7$.
2. Lamb shift corrections and the effect of virtual muon pairs by using the procedure of Barrett[18].
3. Electron screening corrections of Vogel[19].
4. Relativistic center of mass corrections of Fricke[20].
5. Nuclear polarization as calculated by Chen[21] and Vogel and Akylas[22].

Of these corrections, the nuclear polarization contributes the largest effect (-6.8 keV in $1s_{1/2}$ level), as well as the largest uncertainty (1.5 keV). The reader is referred to Appendix A for more details. The results for several muonic energy levels are given in Table 1.

2.2 Hyperfine Interactions

The interaction of the muon with the higher multipole fields of the nucleus (both electric and magnetic) has been discussed extensively in the literature[23,24] and the reader is referred to these articles or to Appendix B. The following is a brief summary of the principal considerations.

In electronic atoms the magnetic hyperfine structure (hfs) is larger or of the same order as the electric quadrupole (E2) hfs with

$$< \frac{\mu_e \mu_N}{r^3} > \gtrsim < \frac{eQ}{r^3} > .$$

In muonic atoms the latter quantity dominates since the muon magnetic moment, μ_μ, is 207 times smaller than μ_e. Both interactions will be covered below in the order of their importance.

2.2.1 Electric Quadrupole (E2) Interaction

The E2 interaction Hamiltonian is given by

$$H_{int}(E2) = \frac{-4\pi}{5} (e^2) \frac{r_<^2}{r_>^3} \sum_m Y^*_{2m}(\theta_N,\phi_N)\, Y_{2m}(\theta_\mu,\phi_\mu) \qquad (2.4)$$

where N(μ) refers to the nuclear (muon) coordinate and $r_{<(>)}$ is the lesser (greater) of the nuclear or muon radial coordinates.

The E2 interaction energy between the muon and the nucleus in the states $|IJ>$ and $|I'J'>$ is

$$\langle IJFM|H_{int}(E2)|I'J'FM\rangle =$$

$$e^2\ (-1)^{J+1/2}\ \left[\frac{4\pi}{5}(2J+1)(2J'+1)\right]^{1/2}\begin{pmatrix} J & 2 & J' \\ 1/2 & 0 & -1/2\end{pmatrix}\begin{Bmatrix} I & J & F \\ J' & I' & 2\end{Bmatrix} \qquad (2.5)$$

$$\times \langle J|\ \frac{f(r_\mu)}{r_\mu^3}\ |J'\rangle\langle I||\Omega^2||I'\rangle$$

where

$\underset{\sim}{F} = \underset{\sim}{I} + \underset{\sim}{J}$ is the total angular momentum of the muon-nucleus system. $f(r)$, denoting the radial integral,

$$f(r_\mu) = 1 - \left\{ \frac{\int_{r_\mu}^{\infty} dr_N \rho_{20}(r) \left(\frac{r_N^5 - r_\mu^5}{r_N}\right)}{\int_0^{\infty} dr_N\ \rho_{20}(r)\ r_N^4} \right\}$$

is a nuclear form factor representing the muon penetration of the nucleus. In the limit of a point quadrupole density, $f(r_\mu) \equiv 1$. The E2 interaction strength is always <u>reduced</u> by muon penetration of $\rho_{20}(r)$. We further introduced the abbreviation

$$\Omega^2 = r_N^2\ Y_{20}(\theta_N).$$

The two quantities in parenthesis and braces are Wigner 3J and 6J coefficients respectively.

The nuclear reduced matrix elements may be related to spectroscopic E2 moments of the various levels (Q_s) and E2 transition probabilities (B(E2)). Q_s is defined by

$$Q_s(I) = e\langle I, M=I | \Omega^2 | I, M=I \rangle$$

$$= e \frac{16\pi}{5} \left[\frac{I(2I-1)}{(2I+1)(I+1)(2I+3)} \right]^{1/2} \langle I || \Omega^2 || I \rangle . \qquad (2.6)$$

The last relation follows from the application of the Wigner-Eckart theorm. The reduced E2 transition probability between the two nuclear states I and I' is related to the reduced nuclear matrix element by

$$B(E2;\ I \rightarrow I') = \frac{e^2}{2I+1} \left| \langle I || \Omega^2 || I' \rangle \right|^2 .$$

2.2.2 Magnetic Dipole (M1) Interaction

The M1 hyperfine energy for the state $|IJF\rangle$ is

$$\Delta W = A_1(I,n,\ell,J) \cdot \left[\frac{F(F+1) - I(I+1) - J(J+1)}{2IJ} \right]$$

with n,ℓ being the muon principal and orbital quantum numbers, respectively. The term in brackets is the familiar angular momentum

term due to $\underset{\sim}{I} \cdot \underset{\sim}{J}$. A_1 is a magnetic nuclear form factor analogous to the factor $\frac{f(r_\mu)}{r^3}$ in equation (2.5). However, unlike the E2 form factor, A_1 is complicated by the fact that the nuclear magnetic moment is composed of two terms, one which is due to the orbital angular momentum, the second to the spin of the nucleus. In general, their radial distributions may be quite different. This feature, known as the Bohr-Weisskopf effect, can either increase or decrease ΔW from point M1 interaction values.

ΔW is largest in the $1s_{1/2}$ muonic level. For the ground state of ^{199}Hg (I = 1/2) we have used the experimental values of Link et al.[25] for A_1 (1/2,1,0,1/2) = 0.117 (29) keV. In ^{201}Hg (I = 3/2) where no experimental value exists, the formulation of Le Bellac[26] was used to calculate A_1 (3/2,1,0,1/2) = -0.166 (17) keV, assuming the magnetic moment is due to a single $p_{3/2}$ neutron. The values of A_1 should be compared to the E2 hfs energies which are typically of the order of 10~20 keV. Therefore allowing A_1 to vary by more than two standard deviations from the above values will introduce negligible uncertainty in the E2 hfs.

2.2.3 Diagonalization of Hamiltonian

In order to analyze the observed hfs, the Hamiltonian (eq. 2.1) with the E2 and M1 interactions is diagonalized in the restricted subspace of states which include only the muon fine structure components

of a given n and ℓ and nuclear states of the same parity as the ground state and of energy less than 500 keV. Since the E2 interaction falls off quite rapidly for increasing n and ℓ, only the 2p, 3p, and 3d muon fine structure components have a non-negligible dynamic mixing effects. Therefore, the diagonalization of the Hamiltonian was carried out only in these states. Table 2 gives the nuclear states for each isotope which were included in the analysis.

2.3 Atomic Cascade

The observables in a muonic spectrum are not only the energies of a given transition, but also the intensities of the transitions. This especially becomes important when there are hyperfine effects and the relative intensities of the components are needed to derive the hfs splitting from the data. Good agreement with experiment is obtained if one assumes, for the ease of calculation, that the muon is captured by the atom in the n = 18 level, statistically populating the angular momentum states. From here the cascade is followed down to the n = 4 level using the computer code of Hüfner which allowed for the Auger emission of K and L shell electrons and radiative muonic electric dipole transitions. The ℓ^{th} order El transition probabilities are given by a generalization of the long wavelength approximation of Devons and Duerdoth[27], with

$$P(E\ell)_{nEF\to n'E'F'} = \frac{2\alpha}{\hbar} mc^2 \left(\frac{E-E'}{mc^2}\right)^{(2\ell+1)} \frac{(\ell+1)}{(2\ell+1)\ell[(2\ell-1)!!]^2} (2F'+1)$$

$$\times \left| \sum_{I\,J\,J'} (-1)^{J+I+F'+\ell} \begin{Bmatrix} J' & F' & I \\ F & J & \ell \end{Bmatrix} \langle J'||M(\ell)||J\rangle \right.$$

$$\left. \langle IJ;F|EF\rangle\langle IJ';F'|E_\beta'F'\rangle \right|^2$$

where $\langle IJ;F|EF\rangle$ is the amplitude of an eigenstate component and

$$\langle J'||M(\ell)||J\rangle = (-1)^{J+1/2}(2J'+1)^{1/2}(2J+1)^{1/2}\begin{pmatrix} J' & J & \ell \\ 1/2 & -1/2 & 0 \end{pmatrix}$$

$$\times \int_0^\infty \left(\frac{r}{\alpha a_o}\right)^{\ell} (ff'+gg')\, r^2 dr$$

with f(g) the large (small) Dirac radial wave function. For all levels with $n > 4$ point nucleus wave functions were chosen. For $n \leq 4$ the Dirac equation was solved with realistic charge distribution to calculate the radial matrix element. For $n \leq 4$ only muonic radiative E1 and E2 transitions were taken into account. This is justified since the nuclear radiative transitions of interest are orders of magnitude slower than the muonic transitions. Thus a given component of a system eigenvector $|JIF\rangle$ can only feed other eigenvector components with $I' = I$.

SECTION 3.0

EXPERIMENTAL SETUP

The data were taken at the muon channel of the Space Radiation Effects Laboratory (SREL) in Newport News, Virginia. Eight targets were exposed simultaneously in the beam. Six of these were enriched mercury isotopes and two were enriched targets of ^{208}Pb. The experimental setup was designed with two goals in mind: (1) the elimination of systematic bias and gain shifts between different isotopes and (2) the efficient use of all the available beam and time allotted to us.

In order to identify eight different targets it was necessary to tag each separately with an identification code. This was done with plastic scintillation counters and fast logic. The muon telescope is shown in Figure 2. Counters 1 and 2 in coincidence define charged particles emerging from the muon channel. Between counters 2 and 3 a polyethylene plastic moderator was used to slow the muons. The total stopping rate was typically 1.9×10^4 sec^{-1}. Figure 3 shows the arrangement of the 3(i) and 4(j) counters and targets (i=1,4;j=1,2). The targets were arranged in two square arrays. The number 3 scintillators determined in which quadrant a muon entered. The number 4 counter determined whether it stopped in the upstream targets or entered the downstream targets. Counter 5 was a veto counter which had raised vertical and horizontal ribs in optical contact with its backplane. Any muon scattering from one target to another would have to

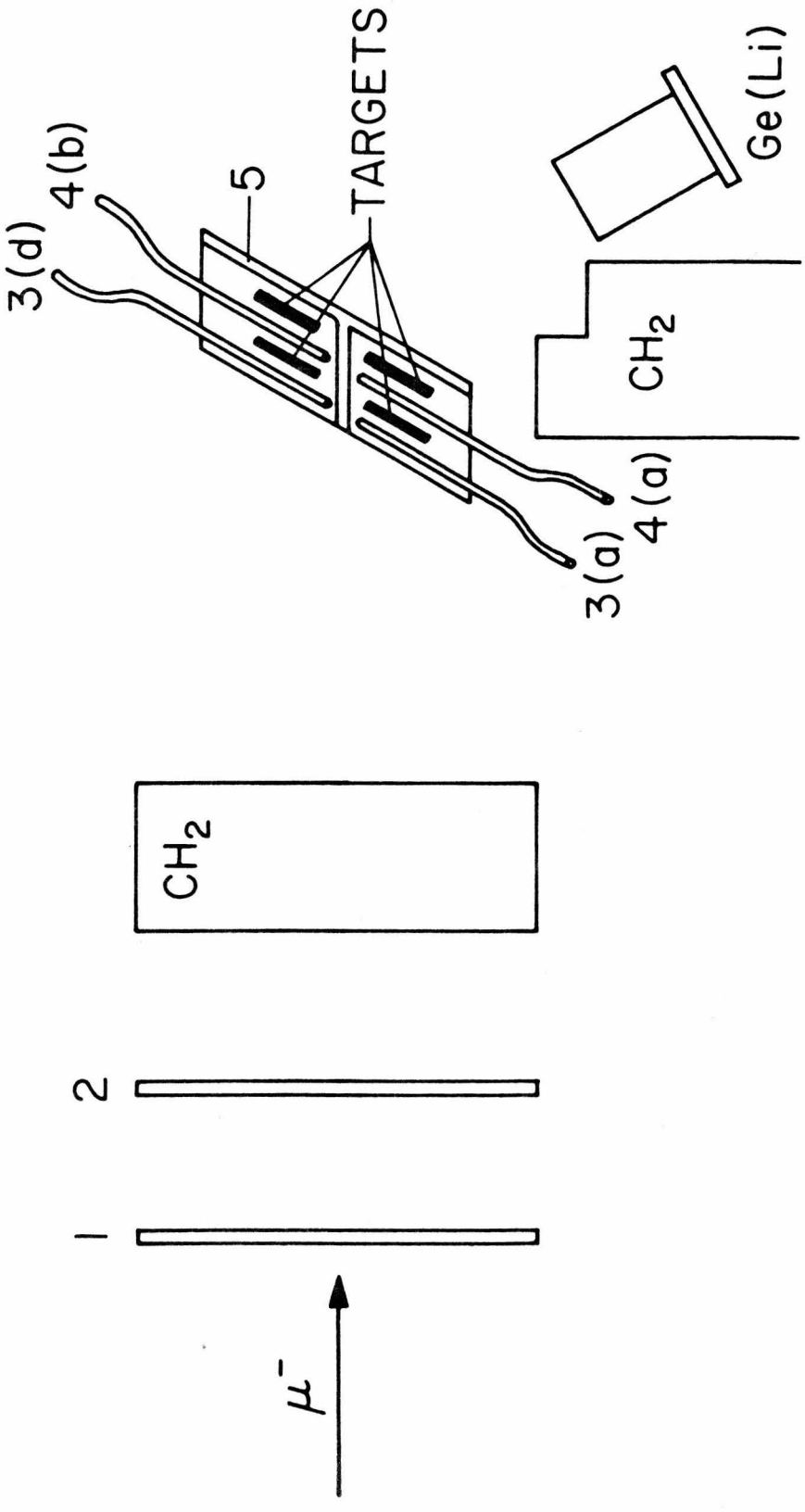

FIGURE 2

Top View of Muon Telescope

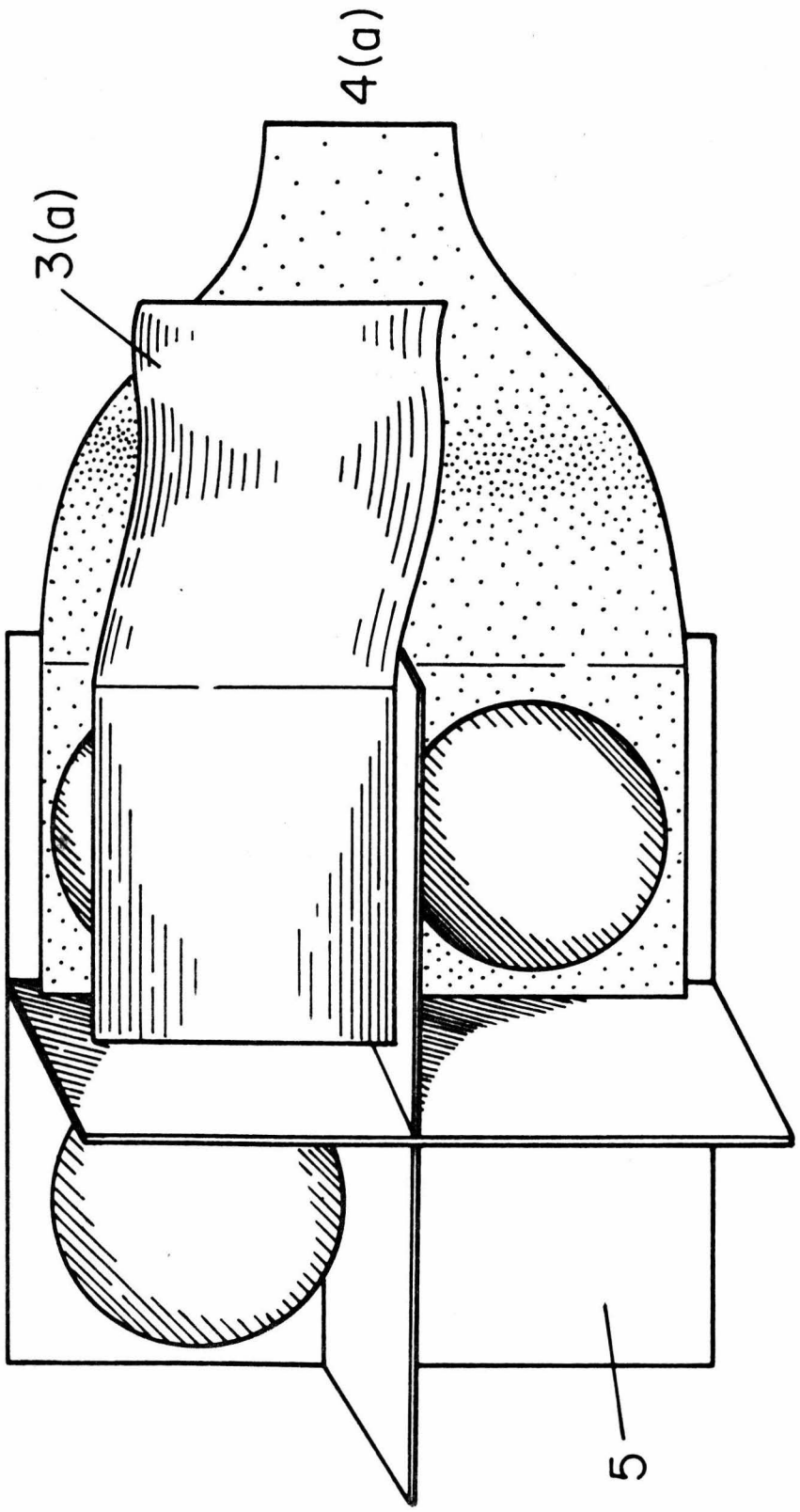

Figure 3
Detail of Target Array

pass through one of these ribs and would be vetoed. A "stop" was characterized by a tagword, either $1 \cdot 2 \cdot 3(i) \cdot \overline{4}(j) \cdot \overline{5}$ for any of the upstream targets or $1 \cdot 2 \cdot 3(i) \cdot 4(j) \cdot \overline{5}$ for the downstream targets.

Each of the Hg isotopes, which were acquired on loan from Oak Ridge National Laboratory, consisted of approximately 2.5 g of enriched HgO. The enrichments along with their physical characteristics are listed in Table 3. The oxide was mixed with 0.8g of Formvar, a plastic, and hydraulically pressed into a pill shape form. The two ^{208}Pb metal targets were each 16 g in mass and at an enrichment of 99.7%. Their shape was similar to that of the Hg targets.

A 100 cm^3 lithium drifted germanium detector (Ge(Li)) manufactured by Princeton Gamma Tech was used in the experiment. This detector exhibited an offbeam energy resolution of 1.7 keV (FWHM) at 1.33 MeV. The energy pulse output was shaped and amplified by a Tennelec TC203BLR amplifier. The amplifier output was digitized by a Kicksort 8192 channel ADC. Detector timing information was used with the muon telescope logic to provide "start" and "stop" signals to a time-to-amplitude converter (TAC). The TAC output was digitized by a 1024 channel IBM ADC.

If a photon enters the Ge(Li) in coincidence with a "stop" signal from the telescope logic, an "event" pulse is generated. The event pulse interrupts the normal online computer operation causing the data input registers from our ADC's and telescope logic interfaces

to be read. For each event three words (16 bit) were read into a buffer area of memory: (1) the identification tag word, (2) the digitized energy signal, and (3) the digitized time signal. When the buffer was filled, the data were written onto a magnetic tape. This technique (also referred to as "list mode") has the advantage of preserving all the digitized raw data allowing the maximum flexibility in the analysis. During the experiment "prompt" histograms for each target with reduced resolution were stored in the core memory of the IBM 360/44 computer in order to serve as an online monitor of the experiment's progress.

The generation of timing information was needed for the following reasons. The timing resolution of our detector system was 16 ns (FWHM), a time long compared to the time associated with the muonic cascade (10^{-16} sec). Thus any muonic x-ray or gamma ray from nuclear deexcitation of levels populated during the cascade would appear as "prompt" events. Other possibilities include nuclear gamma rays from daughter nuclei formed by muon capture on the Hg (or Pb) nucleus and beam unrelated background events. It should be remembered that the nuclear capture time is on the order of 80 ns and thus appear as "delayed" events in the timing spectrum. Figure 4 shows a typical timing spectrum from our detector. The main peak contains prompt events, while the exponential tail contains the delayed events. This whole spectrum is superimposed upon the "accidental" background (which can be seen in the "early" events, i.e. those which have no time correlation with the muon telescope logic).

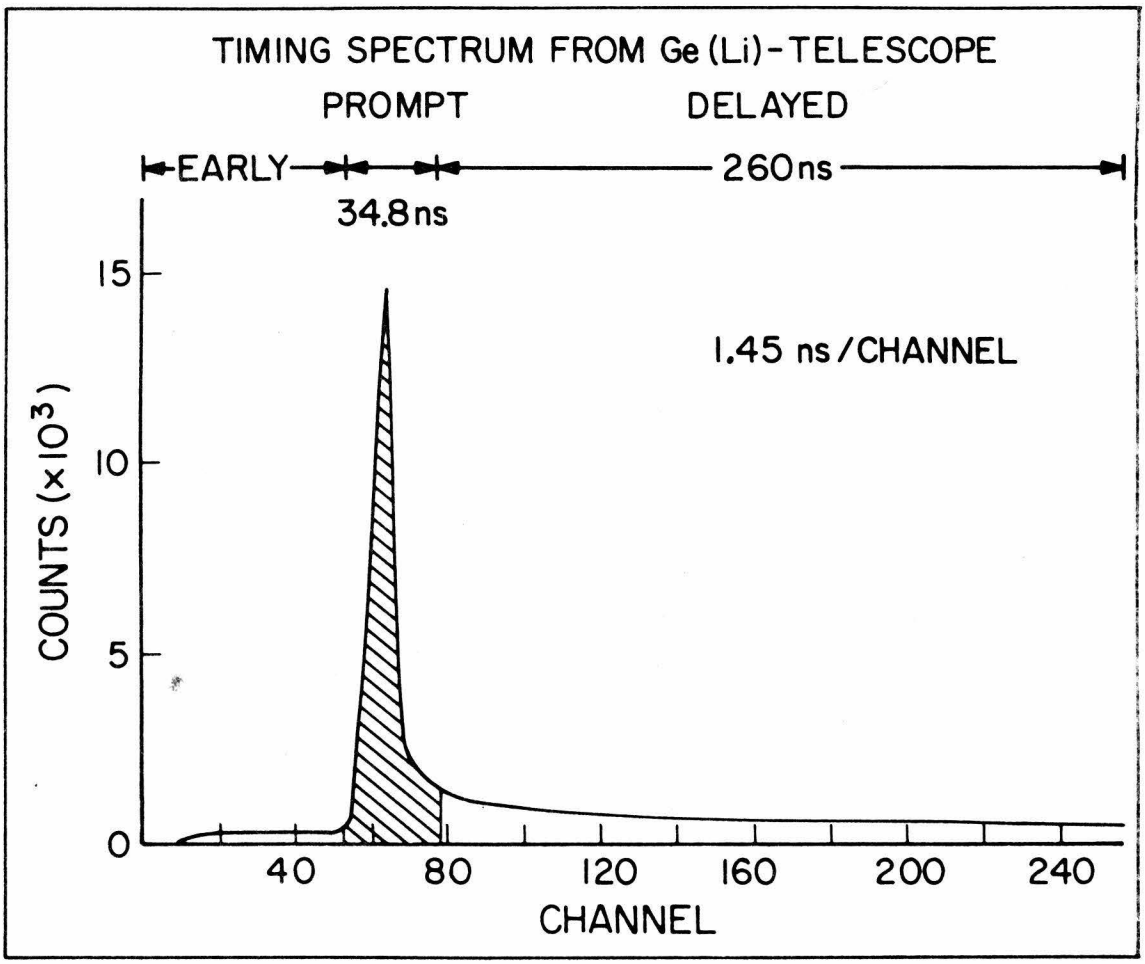
TIMING SPECTRUM FROM Ge(Li)-TELESCOPE
PROMPT
DELAYED
EARLY
260ns
34.8ns
1.45 ns/CHANNEL
COUNTS (×10³)
15
10
5
0
40
80
120
160
200
240
CHANNEL

FIGURE 4

After the online experiment was completed, the magnetic tapes were read back (into the same computer) and 8192 channel energy histograms were formed on disk for both prompt and delayed events for each target. Since the delayed region covers a relatively long period ($\sim$ 260 ns), it contains an appreciable number of accidental events. By searching the delayed spectra any background lines which might interfere with the prompt muonic x-ray transitions could be detected. In our particular case none were found.

3.1 Geometry Effects

It has been noted in references[28,29] that the energy response of a Ge(Li) detector may slightly depend upon the direction of the incoming photon. The magnitude of the effect is dependent upon the individual characteristics of each detector. In general this geometry effect has been found to increase with photon energy. As our targets were at different positions with respect to the Ge(Li), we have investigated this effect by measuring the absolute energies of the (4f$\rightarrow$3d) transitions ($\sim$ 900 keV) and the 511 keV energy differences in the full, single escape and double escape energies of the (2p$\rightarrow$1s) transitions in each quadrant of our target. We have not seen an effect and set an upper limit of 40 eV for the (4f$\rightarrow$3d) transitions and 170 eV for the (2p$\rightarrow$1s) transitions. We have reason to believe that, because of our particular experimental setup in which the detector was pointed

at the center of our square target array, any geometry effect is much smaller than the above limits. The uncertainty introduced by the geometry effect in the determination of the charge parameters of a given isotope is much smaller than that from the theoretical uncertainties. However, for the isotope shifts this uncertainty sometimes equals or exceeds the statistical error. Therefore, in the isotope shift tables we signify which combinations are free of geometry effects by an asterisk.

SECTION 4.0

DATA ANALYSIS

In this section we describe how the charge parameters of the Hg isotopes were extracted from our data. The general energy calibration and peak fitting procedures are given in 4.1. The details which were particular to the analysis in the even and odd isotopes are covered in 4.2 and 4.3 respectively. Finally the model dependence of our analysis is discussed in 4.4.

4.1 Energy and Line Shape Calibration

The ^{208}Pb targets served as both local energy and line shape calibrations for the Hg isotopes since the ^{208}Pb muonic x-ray transition energies are well known[30] and only slightly higher in energy than the corresponding Hg transitions. The ^{208}Pb K(2p→1s) and L(3d→2p) transitions were fitted with an analytic line profile taken from Routti and Prussin[31]. This shape is essentially a Gaussian with a high energy exponential tail. The mathematical form is given by

$$F(x) = A \exp\left[-1/2\left(\frac{x-\mu}{\sigma}\right)^2\right] \text{ for } x \leq \mu + \lambda^2$$

$$= A \exp\left[-\frac{\lambda^2}{\sigma^2}\left(x - \frac{\lambda^2}{2}\right)\right] \text{ for } x \geq \mu + \lambda^2 , \qquad (4.1)$$

where μ is the centroid and σ^2 the variance of the Gaussian portion of the line profile. This function is smooth and continuous through the point $x = \mu + \lambda^2$. The background was approximated by a linear function. In the cases where two or more peaks were fitted over a long region a quadratic background term was also included. The χ^2 values of the fits to the ^{208}Pb K and L transitions were $\leq$ 1.0 per degree of freedom (1.0/DF) and $\approx$ 3.0/DF respectively. The same transitions in the Hg isotopes always had $\chi^2 \leq 1.0$/DF.

We determined the parameters σ and λ for Hg from the Pb fits. This allowed us to unfold the more complex structure seen in the Hg targets (see Figure 5 for a comparison of the Hg and Pb full energy K transitions. The structure in Hg is due in part to contaminations of other Hg isotopes and hyperfine splitting). In particular cases in the Hg isotopes where σ and λ were allowed to vary, the results for these parameters were always consistant with the Pb values (the notable exception of ^{202}Hg is discussed in section 5.3). Since ^{208}Pb served as both an energy and line shape calibration for Hg, there should be no systematic error in the determination of the absolute energies of the Hg isotopes.

In the analysis of the M transitions (4f→3d) it was necessary to modify eq. (4.1) to also allow the inclusion of low energy tails. The reason for this complication was that ^{201}Hg exhibited a 3d hfs. Unfortunately, this structure appeared only as a line broadening. In order to extract $Q_s(3/2)$ and any other dynamic E2 moments responsible

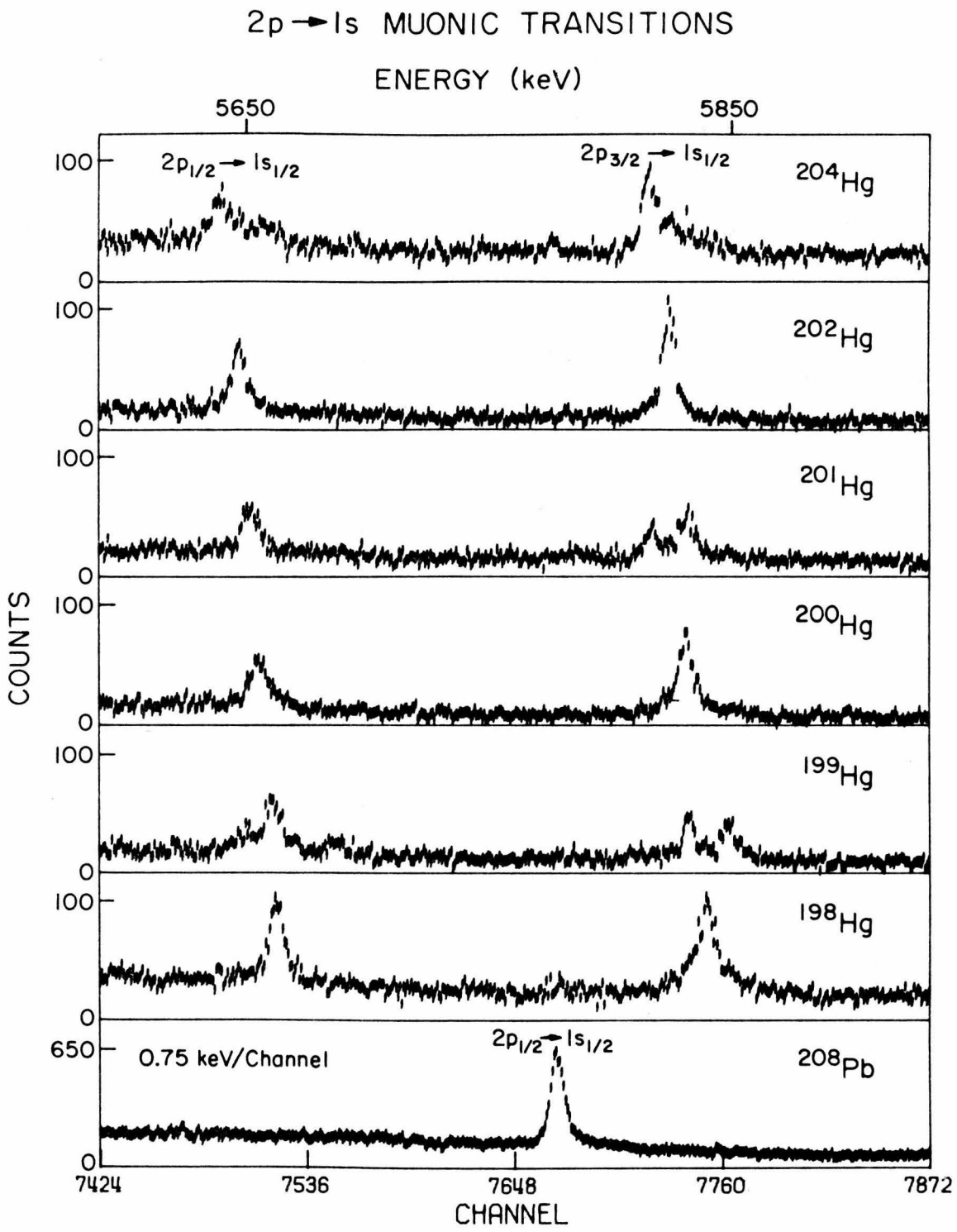

FIGURE 5

Full Energy 2p→1s Muonic Transitions in Hg Isotopes and ^{208}Pb

for the broadening, it was necessary to carefully unfold the M transitions. The peak shape finally chosen was a Gaussian with a low energy tail and two smaller satellite peaks offset at a higher energy to simulate the high energy tail. This shape gave a χ^2 value of 1.4/DF to the Pb M transitions. For the Hg M transitions χ^2 was approximately 0.7/DF. Figures 6 and 7 show the fits to the ^{202}Hg and ^{201}Hg M transitions. The satellite peaks are most easily seen as bumps on the high energy side of the large peaks in ^{202}Hg.

4.2 Even Isotopes

The muonic transitions in the even Hg isotopes, with the exception of ^{202}Hg, exhibited no hyperfine splitting. Hence it was straightforward to find the energies of these peaks. The only complication lay in correcting each target for contributions from impurities from the other isotopes. In the following discussion the word "centroid" is used to mean the parameter μ in eq. (4.1), even though μ is not the centroid of this distribution.

The procedure began with the fitting of a single peak to the transition of interest ignoring any impurities. This constituted the zeroth order centroid. The next iteration used the zeroth order centroids to predict the isotope shift of the impurity peaks. This was done by fixing each impurity centroid to its corresponding zeroth order centroid and setting the relative intensities according to the assay sheets of each isotope. The shift of the first order centroids

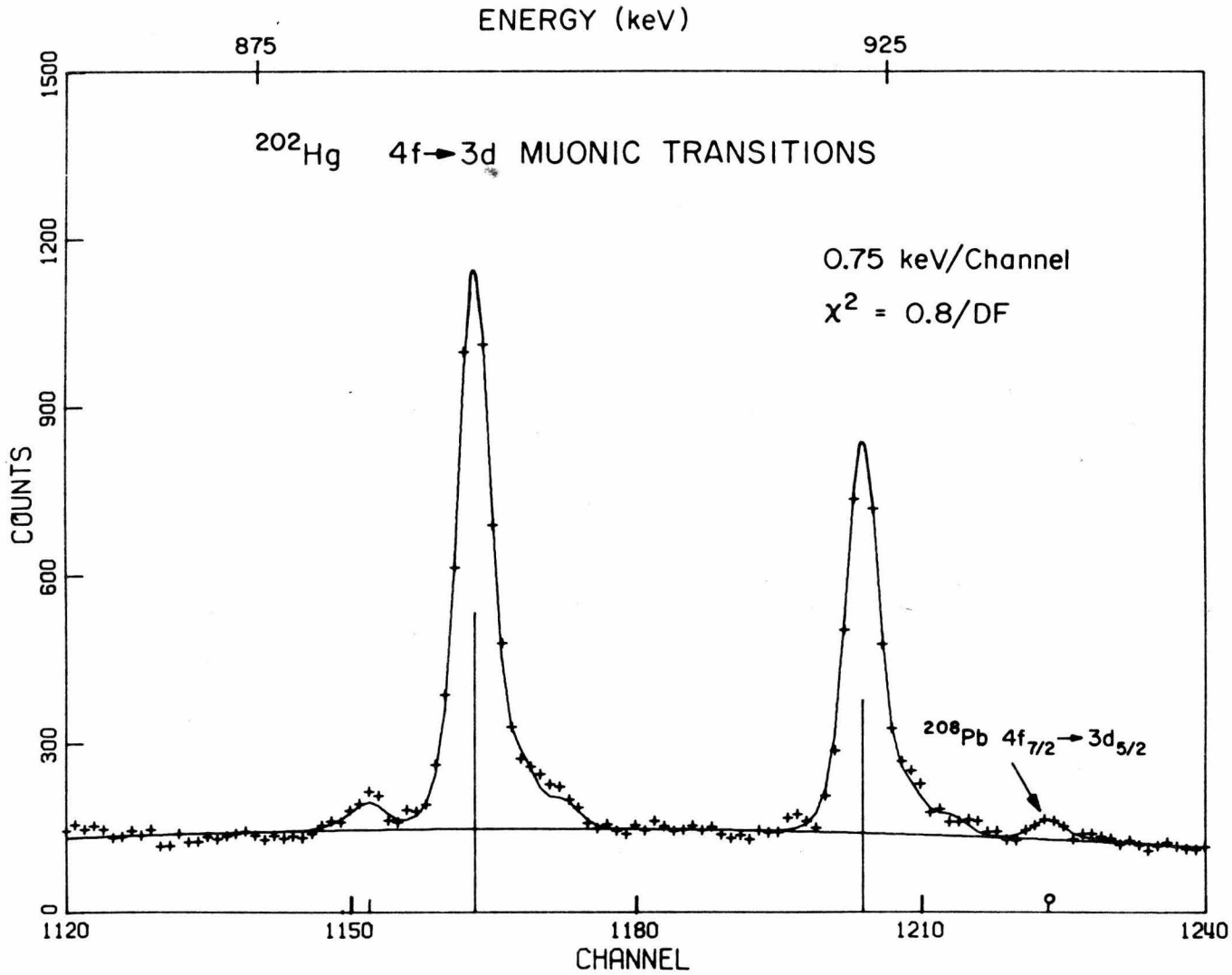

FIGURE 6

^{202}Hg 4f→3d muonic transitions. The solid line illustrates our peak shape. The high energy "bumps" on main lines are the satellite peaks used to simulate the high energy tail. The vertical bars represent relative peak intensities. The vertical bars topped by circles represent contamination peaks.

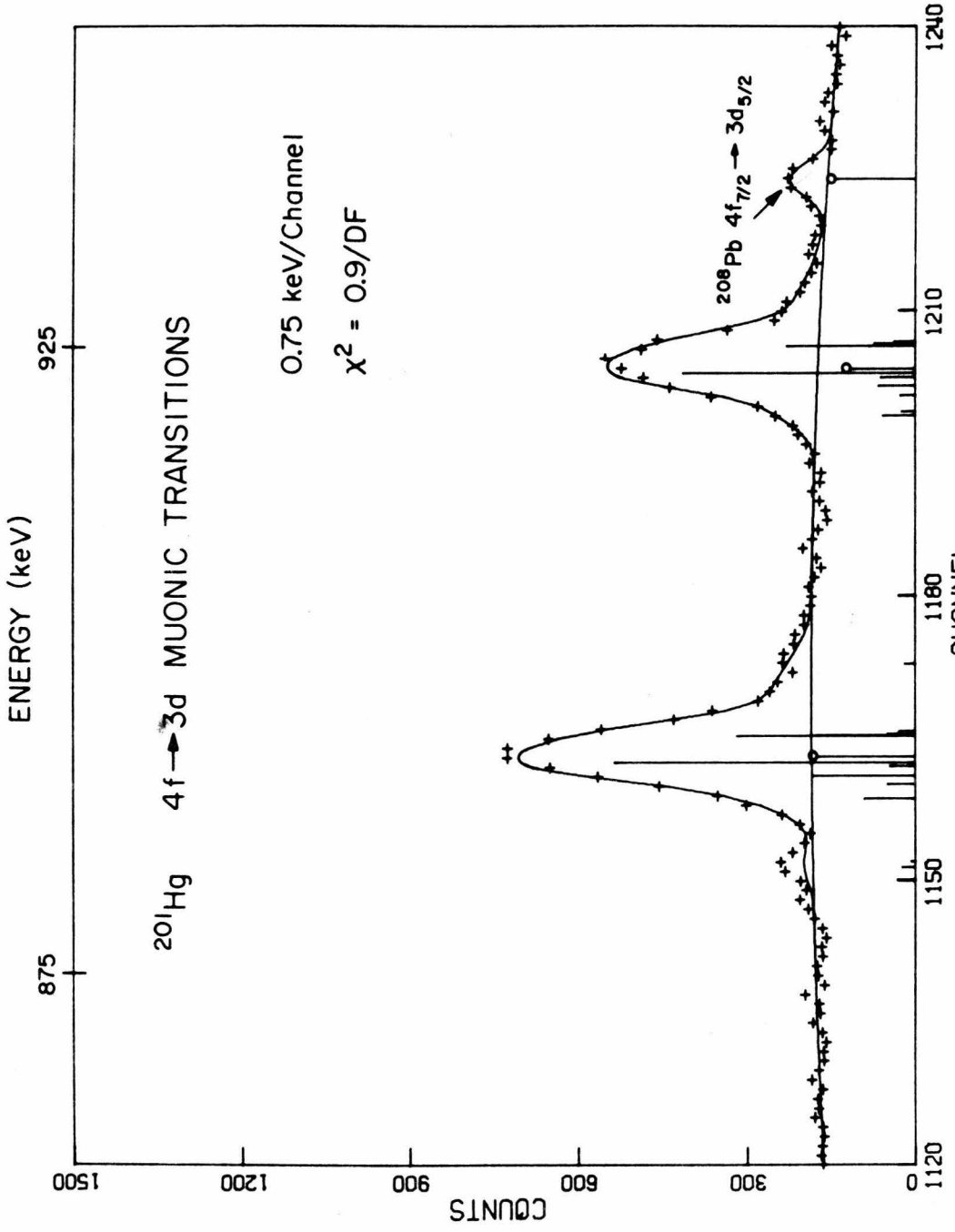

FIGURE 7

^{201}Hg 4f→3d muonic transition showing hfs broadening.

from the zeroth order centroids was small, showing that an iterative procedure would converge very quickly. We only went to the second order and at this point the change of the second order centroid from the first was almost negligible.

The levels which have the most dependence upon the finite nuclear size are the $1s_{1/2}$, $2p_{1/2}$, and $2p_{3/2}$*. Therefore, only the L and K transitions were used in the analysis of the charge distribution. These transitions were also used to derive the 2p fine structure splitting ($\Delta 2p = 2p_{3/2} - 2p_{1/2}$). This quantity is relatively independent of the theoretical uncertainties arising only from the limitations of the available Lamb shift and nuclear polarization calculations (see Section 2.1). If we take an uncertainty of 30%[18,21] for these corrections we find an error of 1.5 keV for the ($2p_{3/2} \rightarrow 1s_{1/2}$) and 0.5 keV for the ($3d_{5/2} \rightarrow 2p_{3/2}$) lines. The similarity of the $2p_{3/2}$ and $2p_{1/2}$ wave functions cause a near cancellation of both corrections and thus the error in $\Delta 2p$ is 0.03 keV. The three statistically independent experimental quantities are the ($2p_{3/2} \rightarrow 1s_{1/2}$) and ($3d_{5/2} \rightarrow 2p_{3/2}$) transitions and $\Delta 2p$. These quantities are listed in Table 4 for the even isotopes.

In fitting the above experimental energies with the energies calculated from a given charge distribution, the experimental errors were folded with the theoretical errors (from nuclear polarization and Lamb shift). The three experimental numbers allow a

*Although the $2s_{1/2}$ level is also sensitive to the nuclear finite size, the weak transitions to and from it could not be observed in our spectra.

two parameter least squares fit. An attempt to fit the even Hg data without any dynamic E2 interaction by varying c and t of (2.3) was unsuccessful. For example, in ^{198}Hg the best fit gave a $\chi^2 = 72/DF$. The next attempt included the dynamic E2 excitation of the first nuclear 2+ state (occuring at approximately 400 keV in the even Hg isotopes). We used the value of B(E2; 0+↔2+) of ^{198}Hg published by Esat et al.[6] to renormalize the B(E2; 0+↔2+) values of Kalish et al.[32] for the remaining even isotopes (the latter values suffer from a normalization to a relatively inprecise (10%) lifetime[32] measurement of the 2+ state in ^{198}Hg). The reader is referred to Table 4 for the renormalized B(E2) values used in our analysis. To further reduce the number of unknowns, the skin thickness t of eq. (2.3) was set equal to 2.30 fm. Our rationale is that Au and Pb experiments, which bracket Hg, determine a t for these elements equal to 2.30 fm to a precision of about 1%[33,34]*.

---

*This is not to say that the skin thickness is exactly 2.30 fm, but instead that with this choice of t, the best fit values of c determine a nuclear shape which will reproduce the low nuclear radial moments to which our data are sensitive. In traditional fits where c and t are allowed to individually vary, these parameters are found to be anti-correlated, that is, an increase in c will be followed by a decrease in t so as to keep the radial R_k moment (see Section 5.7) the same.

The parameters which were varied in the least squares fit were c and $Q_s(2+)$. Our results are given in Section 5. The χ^2 values for our best fits were consistently near zero. We account for this low value by the fact that the nuclear polarization error which dominates the total uncertainty in the K and L transition energies is not a random error and strictly speaking cannot be treated as such. However, we use it to properly weigh the $(2p_{3/2} \rightarrow 1s_{1/2})$ and $(3d_{5/2} \rightarrow 2p_{3/2})$ transition energies in relation to the $\Delta 2p$ energy. The errors quoted for c and $Q_s(2+)$ in Table 4 depend upon the steepness of the χ^2 surface and not upon the magnitude of the χ^2 minimum and therefore are reasonable estimates of the uncertainty in each parameter.

4.3 Odd Isotopes

Since the K and L transitions in both ^{199}Hg and ^{201}Hg are split into many components by the E2 interaction, it was necessary to handle the analysis in a different manner than in the even isotopes. A reasonable value of c was first chosen by using the relative isotope shifts from the optical data[14] to interpolate our results from the adjacent even Hg isotopes. This value of c was used to calculate the unperturbed muonic energy levels. This was possible since the hfs only weakly depends upon the absolute energy of the muonic levels. A computer code, which was individually modified for each isotope, was used to calculate the hfs pattern. By varying $Q_s(I)$ and $B(E2;I \rightarrow I')$

the relative intensities as well as the splittings could be changed. These patterns and their centroids were used to fit the experimental spectrum, again using the Pb peak shape. The best fit centroids from the K and L patterns were then used in computing the half-density radius c.

One difficulty which enters the odd isotope analysis is the relative phases of the off-diagonal (in I) nuclear matrix elements in eq.(2.5). In 3x3 or larger matrices, the determinant has terms sensitive to the overall phase of the product of three or more matrix elements. In ^{199}Hg and ^{201}Hg there are many nuclear states which are connected through these off-diagonal elements leading to many possible combinations. Unless a nuclear model is incorporated to relate these phases and reduce the number of unknowns, a certain ambiguity remains in the analysis. The particular problems in ^{199}Hg and ^{201}Hg are individually discussed in Section 5.

4.4 Model Dependence of the Charge Distribution

Ideally, one would hope that muonic x-rays could provide a "photograph" of the nucleus. As Ford and Wills[35] have shown, each muonic energy level is sensitive only to a particular low order radial moment of the charge distribution. This is the "R_k" analysis which will be discussed in section 5.7. Two charge distributions which have the same low order moments cannot be distinguished by muonic x-rays. Complementary information on the higher order moments is provided by electron scattering experiments. The Fermi-function shape

of eq. (2.2) has been found to satisfy both e^- and μ^- data (e.g. $^{197}Au^{(34)}$).

In the analogous manner, the determination of the angular dependence of the nuclear charge distribution also requires corroborating evidence. With the reasonable assumption that the general E2 charge densities are given by $\rho_{2m}(r) = a_m\rho_2(r)$ (where $\rho(r) = \rho_o(r) + \sum_m \rho_{2m}(r)Y_{2m}(\theta)$ and $\int_o^\infty r^2dr\ \rho_2(r) = 1$), the E2 interaction energy is independent of the intrinsic nuclear coordinate system (this was the underlying assumption for deriving eq. (2.5)). Thus assuming that one can calculate $\rho_2(r)$, the experimental observables $Q_s(I)$ and $B(E2;I\rightarrow I')$ can be related to the intrinsic nuclear coordinate system only through a nuclear model based on an intrinsic set of nuclear parameters. Since eq. (2.5) is general for any electric probing particle it must be concluded that these experiments (μ^-, x-rays, Coulomb excitation, e^- hyperfine interaction, etc.) never directly measure the intrinsic nuclear deformation.

We have made the further simplifying assumption that the same quantity $\rho_2(r)$, describes both the E2 charge density of a single nuclear state and the E2 transition density between two different nuclear states. We have calculated $\rho_2(r)$ from the charge distribution of reference[36]. Figure 8 shows a typical $\rho_o(r)$,$\rho_2(r)$, $\frac{f(r)}{r^3}$, and $r^2\psi^*\cdot\psi$ for the $2p_{3/2}$ and $3d_{3/2}$ muonic states. It can be seen that $\rho_2(r)$ is roughly Gaussian in shape and centered at the half-density radius c. Comparison of the $3d_{3/2}$ and $2p_{3/2}$ densities illustrates the former's relatively small penetration of $\rho_2(r)$. If $Q_s(I)$ can be

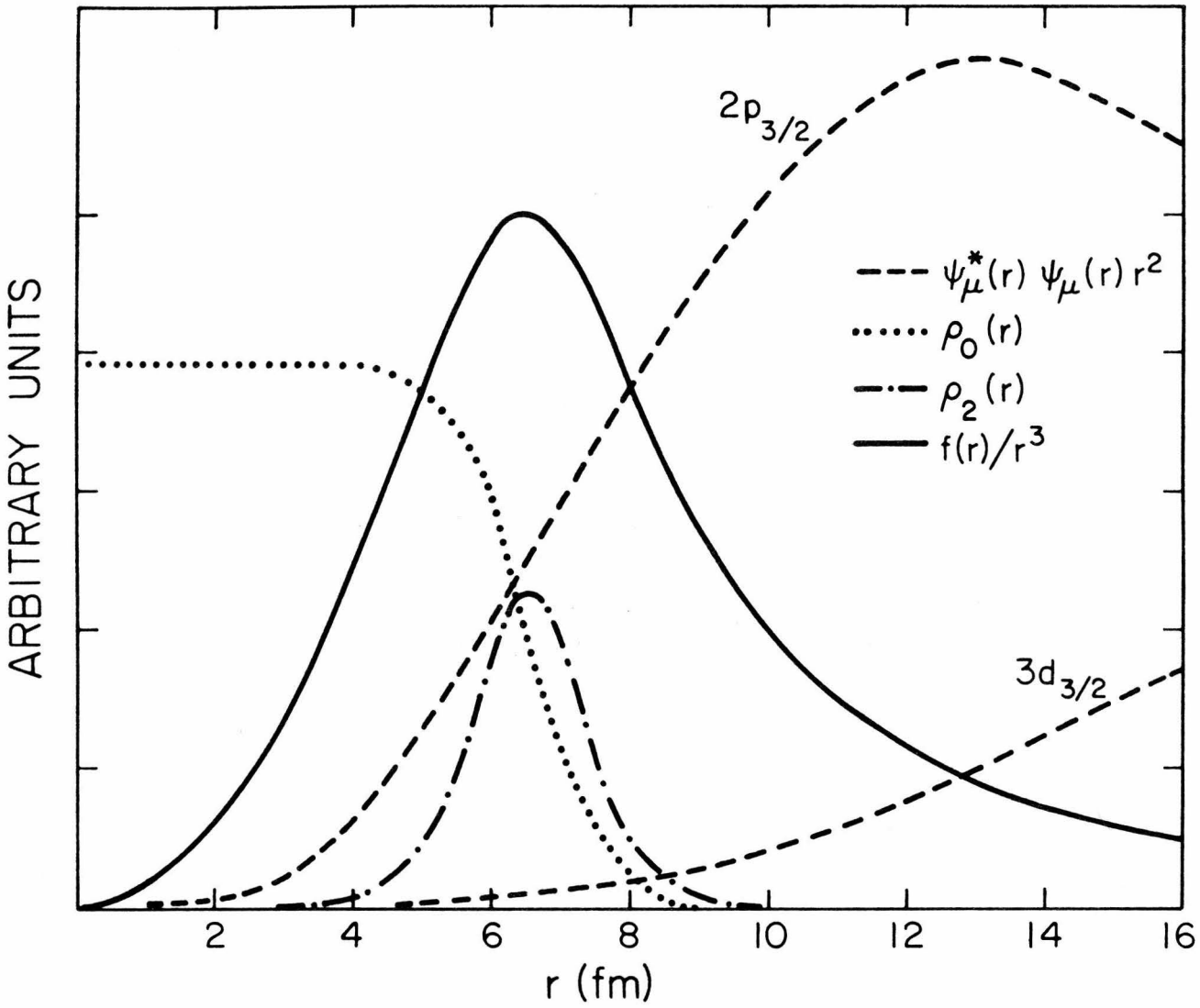

FIGURE 8

Comparison of the $3d_{3/2}$, $2p_{3/2}$ muonic probability densities (weighted by r^2) with the quadrupole penetration function. Also shown are the nuclear monopole and quadrupole charge densities.

measured in the $3d_{3/2}$ and $3d_{5/2}$ levels, as well as the $2p_{3/2}$ state, then the accuracy of $\rho_2(r)$ may be determined. Unfortunately this was not possible in the Hg isotopes, but the results for ^{197}Au (I=3/2) of Powers et al.[33] show at most a 3.6% discrepancy between $Q_s(3/2)$ determined from the 3d hfs and 2p hfs using a similar $\rho_2(r)$. Since some of this discrepancy may result from neglected dynamic E2 excitations[37], we take an uncertainty of 3% for our determination of $\rho_2(r)$. This error has been folded into the statistical errors of all the E2 moments we have determined in the Hg isotopes.

SECTION 5.0

RESULTS

Our experimental energies and the best fit charge parameters for the even isotopes are given in Table 4. Tables 5 and 6 list the results for the odd isotopes, ^{199}Hg and ^{201}Hg respectively. In all cases the values for the half-density radius c are for a spherical Fermi-distribution with a skin thickness t = 2.30 fm. Also listed in these tables are other existing experimental values and theoretical predictions of $Q_s(I)$ and $B(E2;gs\rightarrow I)$. In the following we discuss the problems or procedures pertaining to each isotope.

5.1 ^{198}Hg

Among the even isotopes investigated, ^{198}Hg possess the largest dynamic E2 effect and thus the greatest sensitivity to $Q_s(2+)$. To test the correlation between $Q_s(2+)$ and any possible error in our calculation of $\rho_2(r)$ (which enters through the quantity $\langle j|\frac{f(r)}{r^3}|j'\rangle$ in eq. (2.5)) we arbitrarily increased by 5% the product of $(\frac{f(r)}{r^3})$ and $\langle 2+||\Omega^2||0+\rangle$ in the 2p level and refitted for c and $Q_s(2+)$. The χ^2 value of the resulting fit increased by 1.8/DF but the new fitted values remained within one standard deviation of the original

best fit values. Therefore, we conclude that despite our 3% uncertainty in $\rho_2(r)$, our best fit $Q_s(2+)$ is not materially affected.

After our analysis was concluded another Coulomb excitation experiment by Bockisch et al.[7] came to our attention. It's results severely disagree with both the $B(E2;0+ \rightarrow 2+)$ and $Q_s(2+)$ of Esat et al.[6] for ^{198}Hg. Using the $B(E2;0+ \rightarrow 2+)$ and $Q_s(2+)$ of Esat et al. we tried a one parameter fit of our data varying only c with a resulting $\chi^2 = 0.14/DF$. Then the same procedure was used with the values of Bockisch et al. with a resulting best fit $\chi^2 = 21.0/DF$. We concluded that in the latter experiment, a systematic error must occur in the values of $B(E2;0+ \rightarrow 2+)$ which affects their determination of $Q_s(2+)$. Therefore we disregarded the results of that reference. Our best fit value for $Q_s(2+)$ is slightly inconsistent (but within 1.5 σ) with the more precise value of Esat et al. Both values along with theoretical predictions[3,4,5] are listed in Table 4. We find good agreement between the experimental values and theory.

The comparison of the $(4f_{7/2} \rightarrow 3d_{5/2})$ transition energy with the same transition in the other isotopes shows that the energy in ^{198}Hg is 0.10(4) keV (statistical error given) lower. The $(4f_{5/2} \rightarrow 3d_{3/2})$ transition energy shows no such discrepancy. This may be attributed to a resonance of the $3d_{3/2}$ level similar to that seen by Kessler et al.[34] in the Pb isotopes.

5.2 ^{200}Hg

As can be seen from Table 4 it appears that the Δ2p experimental values as determined by the K and L transitions are inconsistent. The problem appears to be in either the ($3d_{3/2} \rightarrow 2p_{1/2}$) or the ($2p_{1/2} \rightarrow 1s_{1/2}$) transition energies (the corresponding transitions to and from the $2p_{3/2}$ level are ruled out by comparisons with the optical relative isotope shifts. For a more complete explanation see Section 5.7). It is difficult to understand how some equipment failure could affect all three (full energy, single escape, and double escape) ($2p_{1/2} \rightarrow 1s_{1/2}$) peaks and not the three ($2p_{3/2} \rightarrow 1s_{1/2}$) peaks. The most likely explanation is that some mishap occurred with the ($3d_{3/2} \rightarrow 2p_{1/2}$) peak since there is only one of these (only the full energy peak is strong in the L transitions). However, this argument is by no means conclusive and this isotope should be remeasured.

Even with this inconsistency it was still possible to fit c and $Q_s(2+)$ to our data. The error for average Δ2p was increased to 0.44 keV so as to cover both experimental values. The results are listed in Table 4. Our experimental value for $Q_s(2+)$ is slightly inconsistent (within 1.4σ) with theory[3]. In the case of the isotope shifts it was possible to use only the ($3d_{5/2} \rightarrow 2p_{3/2}$) and ($2p_{3/2} \rightarrow 1s_{1/2}$) energies, thus avoiding the aforementioned problem.

5.3 ^{202}Hg

Table 7 lists the differences between the observed ^{202}Hg L and K line widths and those predicted from ^{208}Pb. We note that the ($2p_{1/2} \rightarrow 1s_{1/2}$) and ($3d_{3/2} \rightarrow 2p_{1/2}$) x-ray lines are broadened. The most likely

explanation for this is that the $2p_{1/2}$ level is in resonance with a nuclear level and therefore we postulate the existence of a 1^- nuclear level at an energy near the $(2p_{1/2} \rightarrow 1s_{1/2})$ muonic transition energy (5.65 MeV). Since our data are not sufficient to calculate the specifics of the interaction causing the resonance, only a few observational points will be made.

Due to the E1 interaction, the near degenerate unperturbed $|2p_{1/2},0+\rangle$ and $|1s_{1/2},1-\rangle$ levels mix to form the two system eigenstates

$$\begin{aligned} |1\rangle &= \alpha|2p_{1/2},0+\rangle + \beta|1s_{1/2},1-\rangle \\ |2\rangle &= \beta|2p_{1/2},0+\rangle - \alpha|1s_{1/2},1-\rangle \end{aligned} \tag{5.1}$$

The population of these two states is determined from the muon cascade, primarily from the $|3d_{3/2},0+\rangle$ level. Since muonic transitions connect only eigenstate components with the same nuclear state, the ratio of populating the two states is

$$\left| \frac{|1\rangle}{|2\rangle} \right| = \left| \frac{\alpha}{\beta} \right|^2 \tag{5.2}$$

Therefore the $(3d_{3/2} \rightarrow 2p_{1/2})$ transition constitutes a doublet with relative peak heights given by eq. (5.2) and splitting determined by the strength of the E1 interaction and the degree of degeneracy. The mean energy of the two eigenstates is shifted from the unperturbed

$|2p_{1/2},0+>$ values. The two states can be deexcited via the muonic E1 and nuclear channels. In the former case, both eigenstates are depopulated directly to the $|1s_{1/2},0+>$ ground state. However, in the latter case, the states cannot only deexcite by a nuclear E1 transition to the ground state, but may proceed via a nuclear cascade. We searched our prompt and delayed spectra but could not find any evidence of nuclear gamma rays from this cascade. A nuclear transition would reduce the strength of the total ($2p_{1/2} \rightarrow 1s_{1/2}$) peak area (summed over both eigenstates) in comparison to the ($2p_{3/2} \rightarrow 1s_{1/2}$) peak area. No such reduction was seen. Thus we conclude that the transition depopulating both eigenstates is a muonic transition.

The probability of finding a 1^- nuclear level at 5.65 MeV may be estimated from the level density formula given by Bohr and Mottelson[38] for a Fermi gas. If a 1.60 MeV pairing gap energy in ^{202}Hg is assumed, we calculate the level density to be 0.03 levels/keV (this value is only approximate and strongly dependent upon the pairing gap assumed). This density of 1^- states is not inconsistent with our resonance postulate.

Owing to the presence of the E1 resonance it was not possible to determine $Q_s(2+)$ for ^{202}Hg. We determined c from the ($3d_{5/2} \rightarrow 2p_{3/2}$) and ($2p_{3/2} \rightarrow 1s_{1/2}$) transitions (the $\Delta 2p$ energy could not be used since not only does the resonance split the level, but it also causes a shift of the entire level). It should be noted that despite this exotic resonance, there was no internal inconsistency in our data.

5.4 ^{204}Hg

There are no outstanding problems in this isotope and the analysis is straightforward.

5.5 ^{199}Hg

From the hfs of the muonic (2p→1s) and (3d→2p) transitions we have determined four E2 moments in ^{199}Hg. The L transitions yielded information on all four moments while the K transitions were useful for only the moments associated with the lowest excited state. This is a result of the greater statistical precision of the former transitions compared to the latter.

The nuclear level scheme, given in Table 2, shows the low lying excited states at 158($5/2^-$) keV, 208($3/2^-$) keV, 404($3/2^-$) keV, and 413($5/2^-$) keV. The following moments were derived from a fit to our spectra: $Q_s(158)$, $Q_s(208)$, B(E2;0→158), and B(E2;0→208). The B(E2) values for (158→208), (0→404), (0→413), and (208→413) were set equal to the experimentally derived values given in reference (10). The values for $Q_s(404)$, $Q_s(413)$ and the B(E2)'s, (208→413), (158→404), (158→413) and (208→413) were arbitrarily set equal to zero since their effect upon the muonic hfs is negligible (even the inclusion of the 404 and 413 keV state had only a small effect upon the hfs). The values for the $1s_{1/2}$ isomer shift in the 158 and 208 keV states were taken from [30], as was the M1 hfs in the ground state. The M1 hfs in the 158 and 208 keV states were obtained by scaling the ground state's hfs with the help of the relative magnetic moments.

As mentioned in Section 4.4, the unknown phase of the off-diagonal nuclear matrix elements could pose a problem in the analysis. The smallness of the element between the 158 and 208 keV states and the small effect of the upper states upon the hfs reduced the importance of these terms. A check was made by reversing the sign of

$$\langle 158||\Omega^2||208\rangle$$

after a good fit to the experimental spectrum had been achieved. The fit with the opposite sign did not appreciably change the values of the four moments we allowed to vary.

Our values for the four moments are given in Table 5 along with the previous experimental values for the B(E2)'s and the theoretical predictions of ref.[10]. Our B(E2)'s agreed well with the lifetime data[11], but are slightly inconsistent with the Coulomb excitation values [11]. Our Q_s values do not agree with the theoretical predictions, the most striking aspect being that both our spectroscopic quadrupole moments are positive while the predicted values are opposite in sign.

The centroids of the L and K hfs patterns were used to determine the charge parameter c, which is given in Table 5. Figure 9 shows our best fit to the ^{199}Hg L transitions.

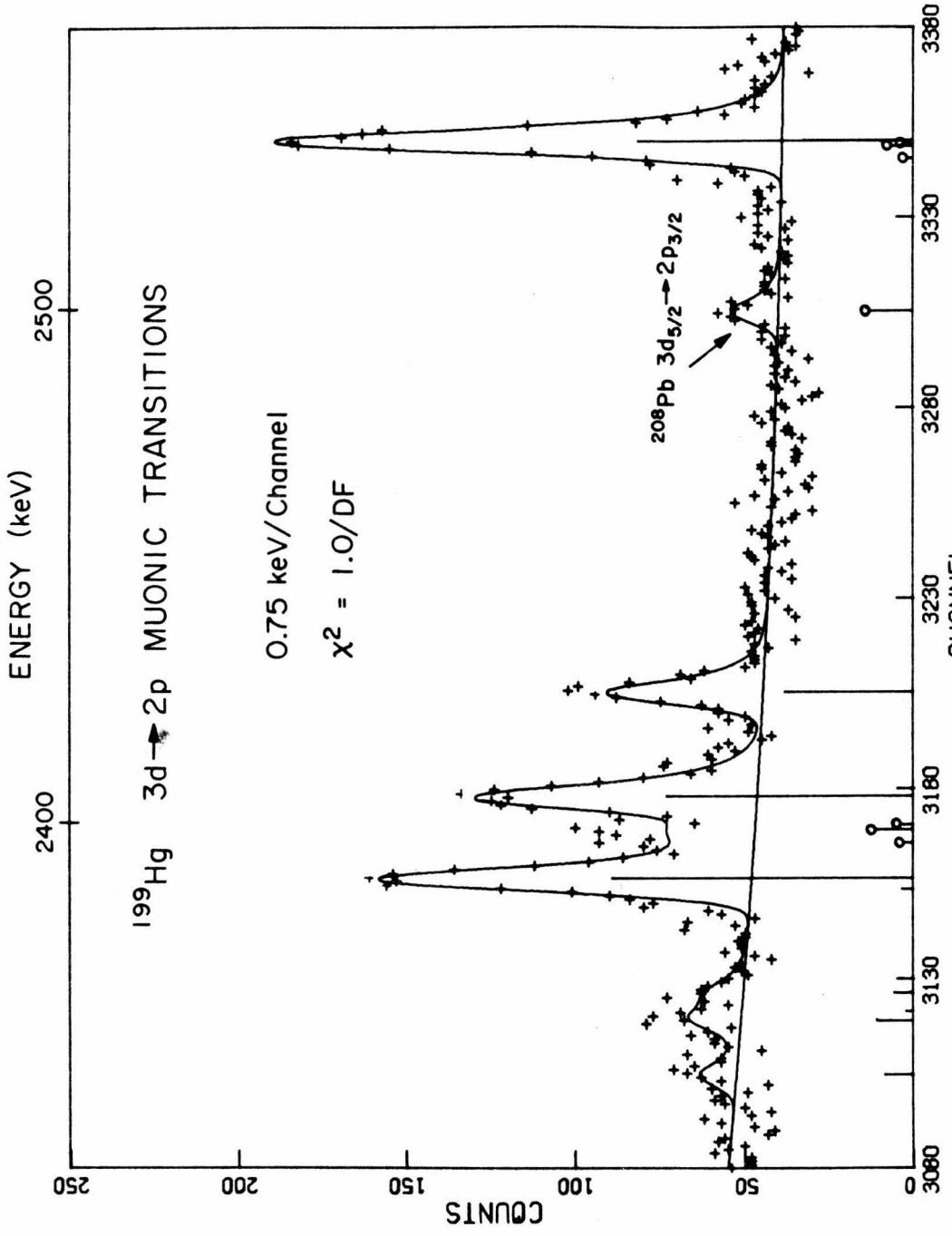

FIGURE 9

^{199}Hg L transition (refer to Figure 7 caption for explanation).

5.6 ^{201}Hg

The best fit to the half-density radius c and the E2 moments are listed in Table 6. The latter quantities are listed by the transitions in which they were determined. $Q_s(3/2)$ of the ground state as determined by the (4f→3d) transitions agrees well with the average of the optical values[39] which have included Sternheimer corrections[40] (polarization of the electron cloud).

The nuclear states included in the hfs analysis are listed in Table 2. The level scheme is taken from Hofmann et al.[12] who have just recently established spin and parity assignments from gamma-gamma correlation studies following the electron capture from ^{201}Tℓ.

As can be seen from Table 6 and Figure 10, three pieces of evidence indicate that our analysis in ^{201}Hg is incomplete. The first is that $Q_s(3/2^-,gs)$ as determined by the L and K transitions is inconsistent with that determined by the M transitions. The second is that the E2 hfs in the L transitions is poorly fit (χ^2 = 1.3/DF compared to 0.9/DF in ^{199}Hg - see Figures 9 and 10). The third piece of evidence is that the energies of the L and K hfs patterns are inconsistent and cannot be fit by our charge distribution by varying c (best fit χ^2 = 18.0/DF as compared to χ^2 = 0.19/DF in ^{199}Hg).

All of these facts might be explained by the omission or misassignment of a nuclear state in ^{201}Hg. Moyer[41] has reported a $5/2^-$ 27 keV state from deuteron pickup and stripping reactions in ^{202}Hg

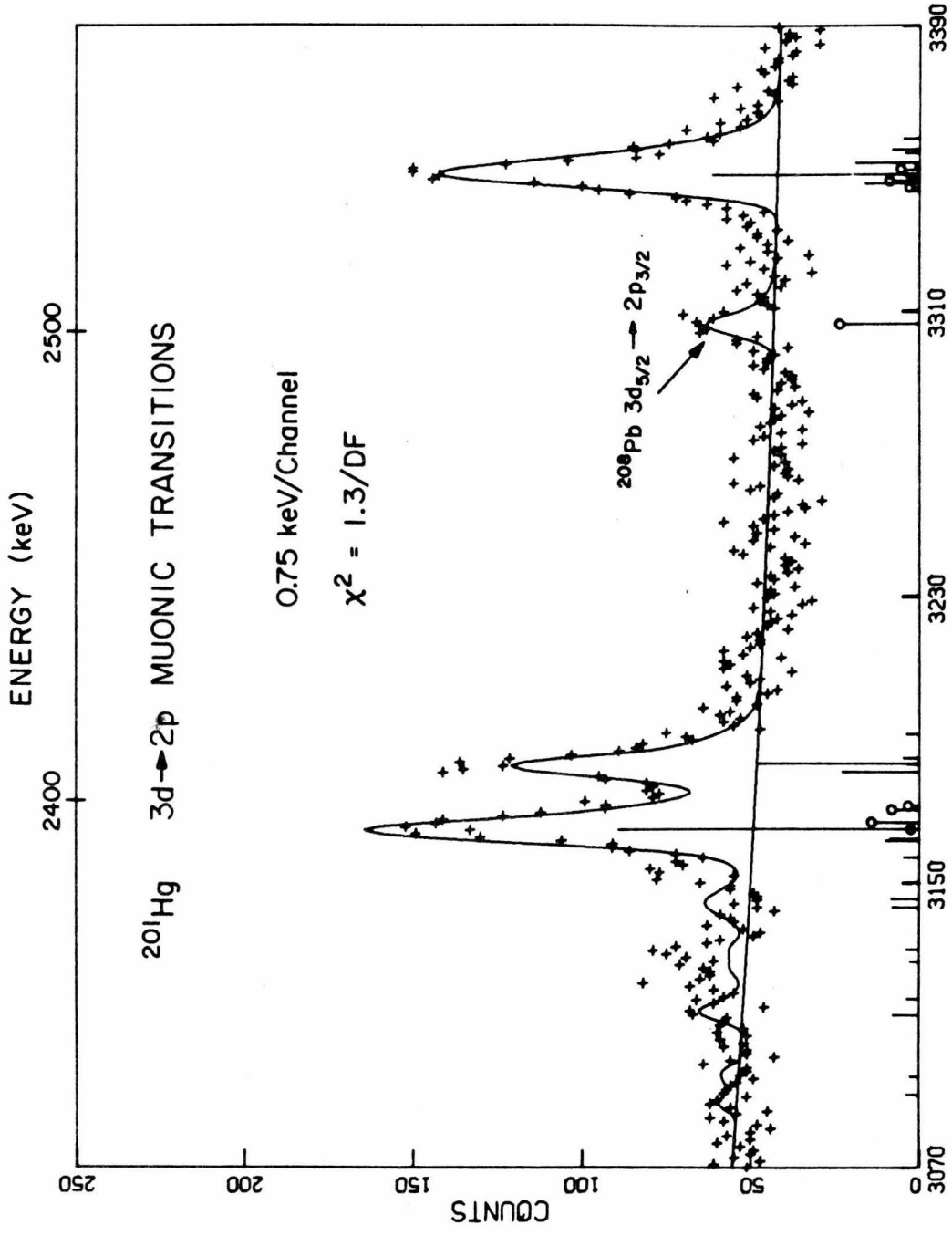

FIGURE 10

^{201}Hg L transition (refer to Figure 7 caption for explanation).

and ^{200}Hg respectively. However, he does not observe the $3/2^-$ 32 keV state. The quoted recent work[12] finds no evidence of this $5/2^-$ 27 keV level. If both experiments are to be consistent with each other, then it must be concluded that the 32 keV $3/2^-$ state is not populated by pickup and stripping reactions and that the opposite situation must be true for the gamma ray cascade following the electron capture decay. It is interesting to note that shell model calculations by Kisslinger and Sorenson[2] predict the ground state spin of ^{201}Hg to be $5/2^-$. It is most likely that a $5/2^-$ level exists in the low energy nuclear levels of ^{201}Hg.

Since nothing definite is known about this $5/2^-$ level we did not attempt a reanalysis of the ^{201}Hg data including such a level. Clearly more nuclear spectroscopic experiments are needed on the level structure of ^{201}Hg before our data or any new muonic data can be unambiguously analyzed.

5.7 Isotope Shifts

Muonic atoms play an important role in the study of isotope shifts. The change in nuclear volume as a result of the addition of neutrons is easily detectable. The "raw" isotope shifts of the K and L transitions do not reflect the actual volume shift since all the effects due to the nuclear E2 moments must first be subtracted. This is obvious for the odd isotopes where the transitions are heavily split up. In the even isotopes the change of the $B(E2;0+ \rightarrow 2+)$ and the 2+ energy from ^{198}Hg to ^{204}Hg is a large effect. To eliminate

the 2p and 3d dynamic interactions we have added the energy of the cascading transitions up to the $4f_{7/2}$ level. At the level of our precision, the 4f level is insensitive to isotope shifts and to any dynamic nuclear effects. In the even isotopes the muonic transitions were summed in two paths:

$$E_1 = (2p_{3/2}\rightarrow 1s_{1/2})+(3d_{5/2}\rightarrow 2p_{3/2})+(4f_{7/2}\rightarrow 3d_{5/2})$$
$$= (4f_{7/2} - 1s_{1/2}) \qquad (5.3)$$

$$E_2 = (2p_{1/2}\rightarrow 1s_{1/2})+(3d_{3/2}\rightarrow 2p_{1/2})+(4f_{5/2}\rightarrow 3d_{3/2})+(4f_{7/2} - 4f_{5/2})$$
$$= (4f_{7/2} - 1s_{1/2}) \qquad (5.4)$$

where $(4f_{7/2} - 4f_{5/2})$ was calculated by our Dirac computer code and the remaining values are experimental measurements. The odd isotopes yielded only one $(4f_{7/2} - 1s_{1/2})$ energy sum since the $(2p_{3/2}\rightarrow 1s_{1/2})$ and $(2p_{1/2}\rightarrow 1s_{1/2})$ transition energies as well as the respective L transitions could not be independently determined.

Table 8 lists the mean $(4f_{7/2} - 1s_{1/2})$ energies (except for ^{200}Hg where both pathways are listed) and the corrections which we applied to the data. The most delicate correction is the change in the nuclear polarization arising from the change in the nuclear deformation. The estimate of the change is relatively straightforward in the even isotopes and was scaled according to B(E2;0+ → 2+) from the

formula of Vogel and Akylas[22]. The odd isotopes were more difficult to handle. In the case of ^{199}Hg the B(E2)'s to all levels were summed with the total being approximately equal to the B(E2;0+ → 2+) of ^{200}Hg. Hence the nuclear polarization correction was taken to be equal to that of ^{200}Hg. Since in ^{201}Hg we could not determine the E2 strength, a B(E2) midway between ^{200}Hg and ^{202}Hg was taken. The error was arbitrarily increased, to 0.2 keV so as to cover both ^{200}Hg and ^{202}Hg values. In addition to the reasons just mentioned, the nuclear polarization is also a function of Z and N. However, it is relatively easy to calculate this change and the reader is referred to Appendix A for a more detailed discussion. Other corrections are due to the changes in the vacuum polarization and the reduced mass of the muon.

Table 9 gives the isotope shift normalized according to the convention:

$$\Delta 1s_{1/2}\ (^{198}\text{Hg} - {}^{204}\text{Hg}) \equiv 3.000 \text{ (arbitrary units)}.$$

Also listed are the relative isotope shifts from optical methods. The precision of the relative optical shifts is much higher than that of the muonic relative shifts and thus they provide severe constraints upon the muonic data. One may immediately notice that in ^{200}Hg only the shift determined by pathway 1 is consistent with the optical values. This implies, as mentioned earlier, that the inconsistency in ^{200}Hg lies in the $(3d_{3/2} \rightarrow 2p_{1/2})$ or $(2p_{1/2} \rightarrow 1s_{1/2})$ lines. The relative values concerning ^{201}Hg are both inconsistent with the optical values and we are unable to offer a simple explanation. One may tentatively attribute the discrepancy

to an error in the nuclear polarization correction in ^{201}Hg since this is the main correction to the isotope shift.

Our interpretation of the isotope shifts in terms of nuclear parameters follows the method developed by Ford and Wills[35] and refined by Barrett[42]. In this analysis the electrostatic potential, V_μ, is derived from the muonic wave function. This potential is parameterized (parameters k and α) in the form

$$V_\mu(r) = A + Be^{-\alpha r} r^k. \tag{5.7}$$

The isotope shift may be written

$$\delta E_{IS} = \delta \int_{\text{Nucleus}} dV_N \rho_o(r_N) V_\mu (r_N)$$

with $\rho_o(r_N)$ the nuclear monopole charge distribution.

In the first order approximation, the muonic wave functions do not change and the isotope shift may be written

$$\begin{aligned} \delta E_{IS} &= A \int dV_N \delta\rho_o(r_N) + B \int dV_N \delta\rho_o(r_N) \{e^{-\alpha r} r^k\} \\ &= \delta\langle Be^{-\alpha r} r^k\rangle \\ &= C_z^{-1} \delta R_k , \end{aligned} \tag{5.8}$$

where

$$\frac{\int_o^{R_k} dV\{Be^{-\alpha r} r^k\}}{\frac{4\pi}{3} R_k^3} = B\langle e^{-\alpha r} r^k\rangle = C_z^{-1} R_k, \tag{5.9}$$

defining the R_k moment as the radius of a uniform charge distribution with the same radial moment as $\rho_o(r_N)$. Engfer et al.[30] have tabulated α, k, and C_z for most nuclei, including Hg. δR_k values have also been calculated for the e^- K x-ray isotope shifts in Hg. This has been done by fitting a curve of the form (5.7) to Seltzer's[43] electronic potential using the same α as in the muonic analysis. The electronic wavefunctions for both e^- K x-rays and optical transitions (which are used in optical isotope shifts) are essentially constant over the nuclear surface and thus they are sensitive to the same R_k moment. Since the e^- K x-ray and optical isotope shifts are traditionally tabulated as $\delta\langle r^2\rangle$ moments, it is necessary to find a coefficient relating δR_k to $\delta\langle r^2\rangle$ in order to facilitate a comparison of the muonic isotope shifts with the electronic values.

We have carried out explicit calculations for R_k in the cases of ^{198}Hg and ^{204}Hg, given the half-density radius c determined by our muonic data, for both R_k values associated with the muonic and electronic $1s_{1/2}$ states. As a function of k we find that δR_k varies less than 0.5% between k = 2.413(μ^-) and k = 2.917 (e^-). Figure 11 shows the μ^- $1s_{1/2}$ and $e^-\delta R_k$'s as a function of k for a selected number of isotope pairs. Table 10 lists the muonic, e^- K x-ray[15], and optical[14] δR_k's for all the possible combinations of isotopes.

In comparing $\delta R_k(\mu^-)$ and $\delta R_k(e^-$ x-ray) we find quite satisfactory agreement. The comparison of $\delta R_k(\mu^-)$ with δR_k(opt) in the even isotopes indicates that the latter values are systematically about 15% larger. We

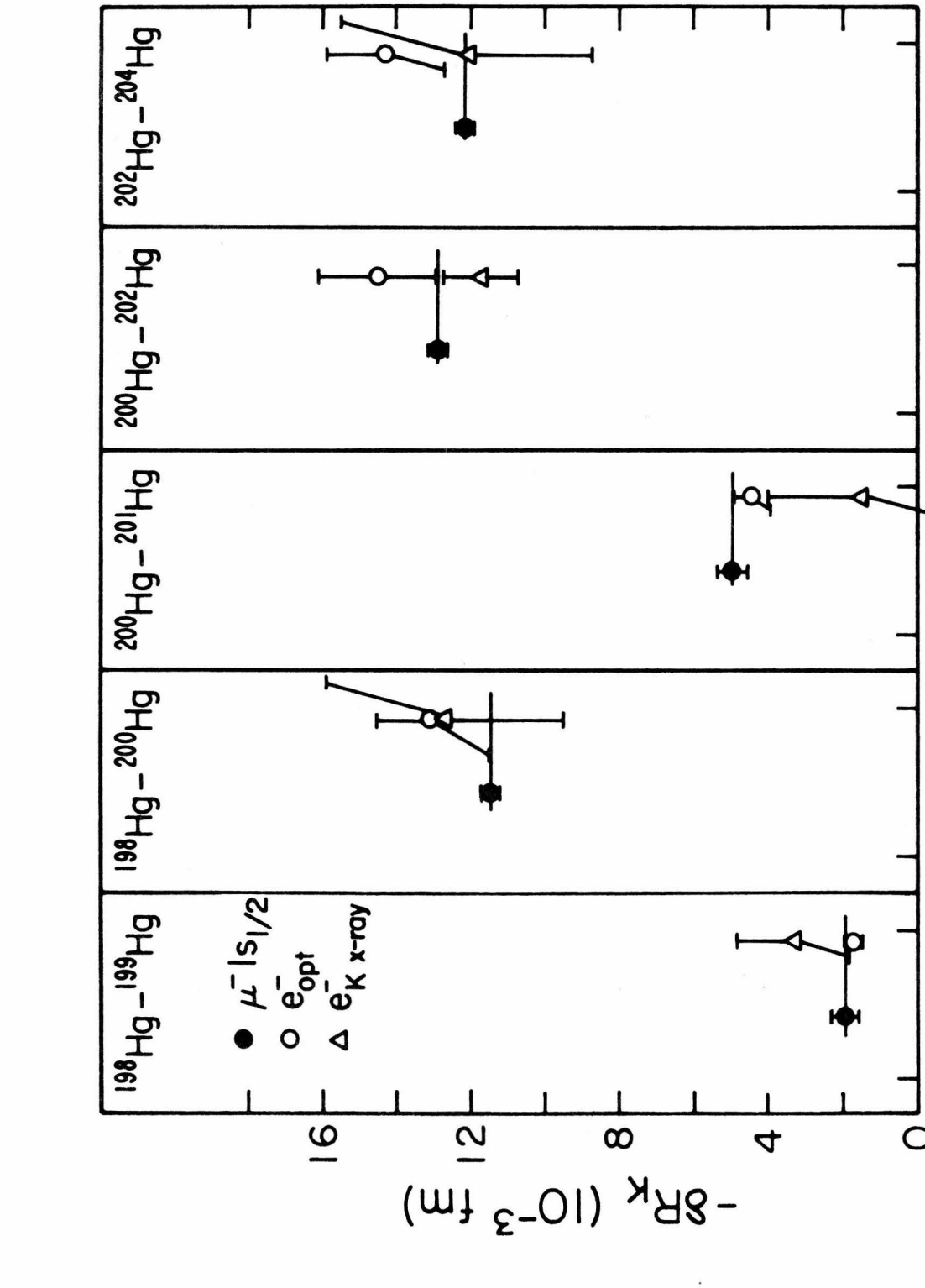

FIGURE 11

Comparison of μ^-, x-ray, e^- x-ray and optical I.S. Solid line is calculated assuming a Fermi distribution for the nuclear monopole charge density.

believe this is a result of a common inaccuracy in the atomic Hartree-Fock (HF) calculations used to convert the optical experimental values into $\delta\langle r^2\rangle$. If we bypass the HF calculations and use the muonic $1s_{1/2}$ isotope shift to directly calibrate the optical shifts we find the conversion factors

$$\delta R_k = -2.354(18) \times 10^{-3} \frac{\text{fm}}{\text{GHz}} \delta\nu \tag{5.10}$$

and

$$\delta\nu = -52.09(38) \frac{\text{GHz}}{\text{fm}^2} \delta\langle r^2\rangle \, . \tag{5.11}$$

In both cases $\delta\nu$ represents the Coulomb field isotope shift in the optical measurements and we have used only the ^{198}Hg - ^{204}Hg μ^- $1s_{1/2}$ shift since it is free from any possible experimental geometry shifts (see Section 3.1). The e^- K x-ray values[15] for (^{198}Hg - ^{204}Hg) and (^{200}Hg - ^{202}Hg) find a conversion factor of

$$\delta\nu = -54.7(3.5) \frac{\text{GHz}}{\text{fm}^2} \delta\langle r^2\rangle \, ,$$

in good agreement with the μ^- results.

SECTION 6.0

OUTLOOK

In this thesis the results from a muonix x-ray experiment in the Hg isotopes have been presented. Except for ^{200}Hg, where an internal inconsistency exists in our data, the limitation in the accuracy of the charge parameters arises not from the experimental errors but rather from the uncertainty in the nuclear polarization calculations. If this uncertainty could be reduced, a great gain in sensitivity to the dynamic E2 excitations and the quadrupole moments, $Q_s(2+)$, in the even isotopes could be achieved. Another limitation comes from the theoretical uncertainty in the E2 charge density ($\rho_2(r)$).

In the case of ^{201}Hg, further progress hinges upon the clarification of the nuclear level scheme. The search for low lying levels in the decays of ^{201}Tℓ and especially ^{201}Au which has not yet been extensively studied, would be a valuable task. Further experimentation using photoproduction of isomeric states in ^{201}Hg[44] also appears to be promising.

In the theoretical domain, the isotope shifts in the entire Hg chain can now be used as sensitive tests for the nuclear Hartree-Fock description. At the present time only a few Hartree-Fock calculations have been published in the Hg isotopes[45] and a complete study, such as carried out for the Sn isotopes[46] would be of interest.

APPENDIX A
NUCLEAR POLARIZATION

The term nuclear polarization traditionally covers all the residual interactions of the muon-nucleus system which are not explicitly included in the normal E2 and M1 hfs analysis. The corrections from the nuclear polarization to the normal interaction matrix element may be calculated in second order perturbation theory by writing

$$\delta M = \sum_{m} \frac{\langle I'j';FM|H_{NP}|m\rangle\langle m|H_{NP}|Ij;FM\rangle}{E_{Ij} - E_{m}} \quad . \tag{A.1}$$

In the particular case where the initial and final states are the same, δM causes a negative level shift since the intermediate states which dominate the summation are much higher in energy than the initial state.

Chen[21] has made detailed nuclear polarization calculations which, in his analysis, the intermediate states conveniently divide into two parts.

$$\langle Ij;FM|H_{NP}|I'j';FM\rangle = \sum_{\ell L} \gamma_{\ell L} A_{\ell L} + \sum_{L} \beta_{L} A_{2L} \tag{A.2}$$

where the $A_{\ell L}$ represent matrix elements which are given by Chen and the $\gamma_{\ell L}$ and β_{L} are functions of the intermediate states. Vogel and Akylas[22] have pointed out that the first term in eq. (A.2) is diagonal in I and j, and thus the net effect is to cause an overall shift

of all the hyperfine components. The second term has off diagonal elements which give rise to a small renormalization (approximately 0.5% in Hg) of the hfs pattern.

Chen[21] provides plots of the $\gamma_{\ell L}$ as a smooth function of Z for the stable nuclei. This is possible since the $\gamma_{\ell L}$ are dominated by the general properties of very high energy (> 10 MeV) nuclear states. Of these states, the giant El nuclear resonances contribute the largest effect. We use this result to calculate how the entire summation over $\gamma_{\ell L}$ varies over the Hg isotopes. It is well known that the giant El strength ($\alpha \sum_i E_i B_i(El)$) and the El level energies are proportional to $\frac{NZ}{A}$ and $A^{-1/3}$ [47] respectively. Referring to eq. (A.1) we find that this part of δM is proportional to

$$\delta M^{El} \alpha \frac{NZ}{A^{1/3}} = \frac{NZ}{(N+Z)^{1/3}} . \qquad (A.3)$$

Since in the Hg isotopes only N changes, the relative change in δM^{El} may be written

$$\frac{\Delta[\delta M^{El}]}{\delta M^{El}} = \frac{2/3\ ZN + Z^2}{ZN(N+Z)} \Delta N.$$

Therefore the change in the $\gamma_{\ell L}$ summation term for the $1s_{1/2}$ muonic level in ($\Delta N = 1$, $N \simeq 122$, $Z = 80$, $\delta M \simeq 6$ keV) is 0.038(12) keV/N, where the error is taken to be 30%[21].

The computer code of Vogel and Akylas has been used to calculate the β_L's for ^{198}Hg. We have used their formalism[22] to extend

these calculations to the other isotopes. As in the preceding case, we assume a 30% uncertainty in these calculations.

APPENDIX B

COULOMB INTERACTION

The classical potential energy of a point electric charge (-e) in a nuclear Coulomb field of charge Ze is

$$V(\underset{\sim}{r}_\mu) = -(e^2)\int_V d^3r_N \frac{\rho_N(\underset{\sim}{r}_N)}{|\underset{\sim}{r}_N - \underset{\sim}{r}_\mu|} , \tag{B.1}$$

where $\mu(N)$ refers to the particle (nuclear) coordinates. Equation (B.1) may be expanded in spherical harmonics and by re-arrangement of the radial integrals be written as

$$V(\underset{\sim}{r}_\mu) = -(e^2) \sum_{\ell} \sum_{m=-\ell}^{\ell} \left(\frac{4\pi}{2\ell+1}\right) q_{\ell m} \frac{f_{\ell m}(r_\mu)}{r_\mu^{\ell+1}} Y_{\ell m}(\theta_\mu, \phi_\mu) , \tag{B.2}$$

where

$$q_{\ell m} = \int_0^\infty \rho_{\ell m}(r_N) r_N^{\ell+2} \, dr_N \tag{B.3}$$

and

$$f_{\ell m}(r_\mu) = \left[1 - \frac{\int_{r_\mu}^{\infty} dr_N \left[\frac{r_N^{2\ell+1} - r_\mu^{2\ell+1}}{r_N^{\ell-1}}\right] \rho_{\ell m}(r_N)}{q_{\ell m}}\right] , \tag{B.4}$$

with $\rho_{\ell m}(r)$ defined by

$$\rho_N(\underset{\sim}{r}_N) = \sum_{\ell,m} \rho_{\ell m}(r_N) Y_{\ell m}(\theta_N, \phi_N).$$

The quantities $q_{\ell m}$ and $f_{\ell m}(r_\mu)$ are the nuclear multipole moments and muon penetration functions, respectively.

B.1 Electric Monopole (E0) Energy

Since monopole excitations of the nucleus are not directly seen in muonic atoms, one may approximate the nucleus by a static charge distribution. The E0 interaction energy is

$$\langle j|H(E0)|j\rangle = -e^2\langle j|\{1-\sqrt{4\pi}\int_{r_\mu}^{\infty} dr_N[r_N^2 - r_\mu r_N]\rho_{00}(r_N)\}|j\rangle .$$

"j" is taken here and elsewhere in this thesis to represent not only the muon angular momentum, but in general all the muon quantum numbers.

B.2 Electric Quadrupole (E2) Energy

The E2 Hamiltonian may be taken from eq. (B.2) and is

$$H(E2) = -e^2\frac{4\pi}{5}\sum_m[r_N^2 Y_{2m}^*(\theta_N,\phi_N)]\frac{f_{2m}(r_\mu)}{r_\mu^3}Y_{2m}(\theta_\mu,\phi_\mu) . \qquad (B.5)$$

The term in brackets has been taken from q_{2m} (i.e. the integral has been "undone"). $f_{2m}(r_\mu)$ is kept in the form as an integral over the nuclear coordinates. If $\rho_{2m}(r) = a_m\rho_2(r)$ (with $\int_0^\infty dr\, r^2\rho_2(r) = 1$) then $f_{2m}(r_\mu)$ is independent of m (cf. eq. B.4 and B.3). That this is true is obvious for axially symmetric nuclei since their deformation is completely characterized by $\rho_{20}(r)$ in the body-fixed axes (with the 3-axis lying along the nuclear symmetry axis). For triaxial nuclei one must admit the possibility

that the $\rho_{2m}(r)$ are not identical in shape. However, in light of the relative incompressibility of nuclear matter, it is still most likely that the quadrupole deformations occur near the nuclear surface and that their respective widths are characteristic of nuclear forces (i.e. one would not expect widely disparate $\rho_{2m}(r)$ shapes in the same nucleus). The accuracy of this assumption is probably consistent with the overall uncertainty ($\sim$ 3%) in calculating an average $\rho_2(r)$.

With the above assumptions, eq. (B.5) becomes

$$H(E2) = -(e^2)\frac{4\pi}{5}\frac{r_N^2}{r_\mu^3} f_2(r_\mu) \sum_m Y^*_{2m}(\theta_N,\phi_N) Y_{2m}(\theta_\mu,\phi_\mu). \tag{B.6}$$

The expectation value of H(E2) is

$$\langle Ij;FM|H(E2)|I'j';Fm\rangle =$$

$$(-1)^{I'+F+3/2}(e^2)\left[\frac{4\pi}{5}(2j+1)(2j'+1)\right]^{1/2}\begin{pmatrix} j & 2 & j' \\ 1/2 & 0 & -1/2\end{pmatrix}\begin{Bmatrix} I & j & F \\ j' & I' & 2\end{Bmatrix}$$

$$\cdot \langle j|\frac{f_2(r_\mu)}{r_\mu^3}|j'\rangle\langle I||r_N^2 Y_2(\theta_N,\phi_N)||I'\rangle \tag{B.7}$$

where I(j) is the nuclear (muonic) angular momentum, F is the total angular momentum of the muon-nucleus system, and M is the projection of F upon the 3-axis. Use has been made of the fact that

$$\sum_m Y^*_{2m}(\theta_N,\phi_N)\, Y_{2m}(\theta_\mu,\phi_\mu) = \underset{\sim}{Y}_2(\theta_N,\phi_N)\cdot \underset{\sim}{Y}_2(\theta_\mu,\phi_\mu)$$

is the scalar dot product of two irreducible tensor operators belonging to independent vector spaces (see equation (3.18) reference[48]) and

$$\langle j||Y^2(\theta_\mu,\phi_\mu)||j'\rangle = (-1)^{j+1/2}\left[\frac{5}{4\pi}(2j+1)(2j'+1)\right]^{1/2} \cdot \begin{pmatrix} j & 2 & j' \\ 1/2 & 0 & -1/2 \end{pmatrix}^{(48)} .$$

REFERENCES

1. H. L. Acker, G. Backenstoss, C. Daum, J. C. Sens, and S. A. DeWit, Nucl. Phys. 87, 1 (1967) 657.

2. L. S. Kisslinger and R. A. Sorenson, Rev. Mod. Phys. 35 4 (1963) 853.

3. A. Covello and G. Sartoris, Nucl. Phys. A104 (1967) 189.

4. K. Kumar and M. Baranger, Nucl. Phys. A110 (1968) 529.

5. T. Kishimoto and T. Tamura, Nucl. Phys. A270 (1976) 317.

6. M. T. Esat, A. M. Baxter, M. P. Fewell, D. C. Kean, and R. H. Spear, Bull. Am. Phys. Soc. 22 4 (1977) 546.

7. A. Bockisch, K. Bharuth-Ram, A. M. Kleinfeld, and K. P. Lieb,

   Proceedings of the Fourth International Conference on Hyperfine Interactions (1977) 48.

8. A. DeShalit, Phys. Rev. 122 5 (1961) 1530.

9. R. Kalish and A. Gal, Nucl. Phys. A175 (1971) 652.

10. G. J. Mathews, F. M. Bernthal and J. D. Immele, Phys. Rev. C 11 2 (1975) 587.

11. R. Kalish, R. R. Borchers, H. W. Kugel, and references therein, Nucl. Phys. A161 (1970) 637.

12. S. Hofmann and D. Walcher, Z. Physik A272 (1975) 351.

13. J. Bonn, G. Huber, H.-J. Kluge, L. Kugler, and E. W. Otten, Phys. Lett. 38B (1972) 308.

14. K. Heilig and A. Steudel, Atomic Data and Nuclear Data Tables, 14 (1974) 613.

15. P. L. Lee, F. Boehm, and A. A. Hahn, Bull. Am. Phys. Soc. 20 (1975) 1496.

16. C. S. Wu and L. Wilets, Annu. Rev. of Nucl. Sci. 19 (1969) 527.

17. J. Blomqvist, Nucl. Phys. B48 (1972) 95.

REFERENCES (continued)

18. R. C. Barrett, S. J. Brodsky, G. W. Erickson, and M. H. Goldhaber, Phys. Rev. 166 5 (1968) 1589.

19. P. Vogel, Phys. Rev. A7 (1973) 63.

20. B. Fricke, Phys. Rev. Lett. 30 4 (1973) 119.

21. M-Y. Chen, Phys. Rev. C. 1 4 (1970) 1176.

22. P. Vogel, V. R. Akylas, Nucl. Phys. A276 (1977) 466.

23. B. A. Jacobsohn, Phys. Rev. 96 6 (1954) 1637.

24. L. Wilets, KGL. Danske Videnskab. Selskab, Mat.-Fys. Medd. 29 3 (1954).

25. R. Link, Z. Physik. 269 (1974) 163.

26. M. Le Bellac, Nucl. Phys. 40 (1963) 645.

27. S. Devons and I. Duerdoth, Adv. Nucl. Phys. 2 (1963) 340.

28. F. C. Roehmer, Helv. Phys. Acta. 45 (1972) 936.

29. P. C. Lichtenberger and I. K. MacKenzie, Nucl. Inst. 116 (1974) 177.

30. R. Engfer, H. Schneuwly, J. L. Vuilleumier, H. K. Walter, and A. Zehnder, Atomic Data and Nuclear Data Tables 14 (1974) 509.

31. J. T. Routti and S. G. Prussin, Nucl. Inst. 72 (1969) 125.

32. R. Kalish, R. R. Borchers, H. W. Kugel and references therein, Nucl. Phys. A147 (1970) 161.

33. R. J. Powers, P. Martin, G. H. Miller, R. E. Welsh, and D. A. Jenkins, Nucl. Phys. A230 (1974) 413.

34. D. Kessler, H. Mes, A. C. Thompson, H. L. Anderson, M. S. Dixit, C. K. Hargrove, and R. J. McKee, Phys. Rev. C 11 5 (1975) 1719.

35. K. W. Ford and J. G. Wills, Phys. Rev. 185 4 (1969) 1429.

36. R. J. Powers, F. Boehm, A. A. Hahn, J. P. Miller, J-L. Vuilleumier, K-C. Wang, A. Zehnder, A. R. Kunselman, and P. Roberson. to be published.

REFERENCES (continued)

37. R. J. Powers, private communication.

38. A. Bohr and B. R. Mottelson, Nuclear Structure Vol. 1 (1969), eq. (2-46), 153.

39. K. Murakawa, J. Phys. Soc. Japan 20 (1965) 1094.

40. R. M. Sternheimer, Phys. Rev. 80 (1950) 102; 84 (1951) 244; 86 (1952) 316; 95 (1954) 736; 105 (1957) 158; 164 (1967) 10.

41. R. A. Moyer, Phys. Rev. C 5 5 (1972) 1678.

42. R. C. Barrett, Phys. Lett. 33B 6 (1970) 388.

43. E. C. Seltzer, Phys. Rev. 188 4 (1969) 1916.

44. J. Vyttenhove and J. Demuynck, Nucl. Inst. 136 (1976) 529.

45. M. Beiner and R. J. Lombard, Phys. Lett. 47B 5 (1973) 399.

46. X. Campi, Nuclear Self-Consistent Fields, (1975) 271.

47. A. Bohr and B. R. Mottelson, Nuclear Structure, Vol. 2 (1975) 478 eq. (6-310); 476 Figure (6-19).

48. M. Rotenberg, R. Bivens, N. Metropolis, and J. K. Wooten, The 3-J and 6-J Symbols, (1959) 23, eq. (3.18); 6, equation for half-integer j.

49. J. Bonn, G. Huber, H.-J. Kluge and E. W. Otten, Z. Physik, A276 (1976) 203.

TABLES

TABLE 1

Theoretical Solutions and Corrections to Dirac Equation for Muonic ^{198}Hg
(Nuclear polarization excluded)
(keV)

Level	Solutions to Dirac Equation m_μ = 105.6594 MeV		Higher Order Vacuum Polarization	Lamb Shift and Anomalous Muon Mag. Moment	Electron Screening	Total Relativistic Center of Mass Motion	Total
	Point Nucleus	Finite Nucleus[a] (incl. 1st order vac. pol.)					
$1s_{1/2}$	19873.890	10263.318	-0.338	-2.724	0.003	-2.519	10257.740
$2p_{1/2}$	5091.129	4597.705	-0.257	-0.325	0.010	-2.110	4595.022
$2p_{3/2}$	4601.397	4422.861	-0.249	-0.609	0.011	-2.188	4419.826
$3d_{3/2}$	2060.103	2066.814	-0.141	-0.040	0.032	-1.167	2065.578
$3d_{5/2}$	2019.841	2027.963	-0.137	-0.045	0.033	-1.150	2026.665
$4f_{5/2}$	1139.571	1143.111	-0.077	0.011	0.079	0.649	1142.476
$4f_{7/2}$	1131.358	1134.807	-0.076	-0.008	0.081	0.645	1134.160

[a]Two parameter Fermi distributions with c = 6.5712 fm, t = 2.3 fm

TABLE 2

Nuclear States of Mercury Isotopes Included in Analysis

	198	199	200	201	202	204
Ground State	(0+)	($1/2^-$)	(0+)	($3/2^-$)	(0+)	(0+)
1	411.8(2+)	158.37($5/2^-$)	367.97(2+)	1.58($1/2^-$)	439.4(2+)	436.8(2+)
2	1048.5(4+)	208.20($3/2^-$)	947.31(4+)	32.19($3/2^-$)		
3		403.4($3/2^-$)		167.49($1/2^-$)		
4		413.5($5/2^-$)				

TABLE 3

Physical Properties of Mercury Targets

Target	Mass(g) (HgO)	Isotopic Analysis 198	199	200	201	202	204
198	2.50	0.7168	0.2202	0.0386	0.0100	0.0124	0.0020
199	2.50	0.0158	0.9148	0.0497	0.0076	0.0105	0.0016
200	2.75	0.0249	0.0614	0.7541	0.0572	0.0903	0.0123
201	2.50	0.0016	0.0036	0.0220	0.9234	0.0477	0.0017
202	2.75	0.0006	0.0017	0.0053	0.0138	0.9758	0.0028
204	2.50	0.0366	0.0612	0.0829	0.0499	0.128	0.642

TABLE 4

Summary of Experimental Energies* and Charge Distribution Parameters for the Even Isotopes

	^{198}Hg	^{200}Hg	^{202}Hg	^{204}Hg
$(2p_{3/2} \rightarrow 1s_{1/2})$	5839.37(12)(52)	5831.19(11)(52)	5824.08(08)(52)	5815.83(13)(52)
$(2p_{1/2} \rightarrow 1s_{1/2})$	5665.89(16)(52)	5658.44(16)(52)	5649.95(14)(52)	5642.36(20)(54)
$(3d_{5/2} \rightarrow 2p_{3/2})$	2398.98(10)(17)	2398.16(10)(17)	2395.49(08)(16)	2394.15(12)(19)
$(3d_{3/2} \rightarrow 2p_{1/2})$	2533.28(14)(20)	2532.62(14)(20)	2530.34(12)(19)	2528.83(17)(22)
$\Delta 2p$(keV)	173.40(13)	172.75(19)K 173.37(17)L	174.00(11)	173.52(16)
c(fm)	6.5712(20)	6.5829(23)	6.5962(23)	6.6181(24)
R_k(fm)[c]	6.9692(21)	6.9801(24)	6.9925(24)	7.0128(25)
$\langle \frac{f(r)}{r^3} \rangle_{2p_{3/2}}$ (fm^{-3})	0.0555	0.0552	0.0550	0.0549
B(E2;0→2)(e^2b^2)	0.981(004)[a]	0.90(06)[b]	0.62(03)[b]	0.35(02)[b]
Q_s(2+) (eb) This exp	0.52(23)	2.6(1.4)	-	0.1(1.7)
a)	0.85(07)	-	-	-
d)	0.75	0.68	0.58	-
e)	0.699	-	-	-

[a] Esat et al.[6]

[b] Values of Kalish et al.[32] normalized to B(E2(0+ → 2+) of Esat et al.

[c] k=2.413 .

[d] Reference[3].

[e] Reference[5].

*First error represents a statistical error in fitting data. Second error includes absolute calibration error.

TABLE 5

^{199}Hg Charge Distribution Parameters

		This Experiment	Coulomb[a] Excitation	Lifetime[b]	Theory[c]
c [d]	(fm)	6.5730(24)			
R_k	(fm)	6.9709(25)			
$\langle \frac{f(r)}{r^3} \rangle_{2p_{3/2}}$	(fm^{-3})	0.0553			
B(E2;1/2→5/2;158 keV)	(e^2b^2)	0.370(09)(24)*		0.375(17)	0.225
Q_s(5/2; 158 keV)	(eb)	0.94(04)(09)*			-0.74
B(E2;1/2→3/2; 208 keV)	(e^2b^2)	0.214(07)(17)*	0.248(15)[e]	0.21(02)	0.246
Q_s(3/2; 208 keV)	(eb)	0.63(15)(15)*			0.46
$\left(\frac{B(E2;1/2\rightarrow 3/2)}{B(E2;1/2\rightarrow 5/2)}\right)$		0.578(33)	0.661(30)	0.56(06)	

[a] Reference (11)

[b] Mean values compiled by Reference (11).

[c] Theory II from Reference (10).

[d] k=2.413 .

[e] Normalized to B(E2;1/2→5/2; 158 keV) from lifetime measurements.

*First error is statistical, second error includes estimated 3% uncertainty in $\langle \frac{f(r)}{r^3} \rangle_{2p}$.

TABLE 6

^{201}Hg Charge Distribution Parameters

		M Transitions	L & K Transitions	Optical
c	(fm)	-	6.5894(24)[a]	
R_k	(fm)		6.9861(25)	
$\langle \frac{f(r)}{r^3} \rangle_{2p_{3/2}}$	(fm^{-3})		0.0551	
Q_s(3/2;gs)	(eb)	0.369(56)	0.176(22)*	0.42[c]
B(E2;3/2→1/2;1.58 keV)	(e^2b^2)	0.110(23)	0.113(08)*	
B(E2;3/2→3/2;32.19 keV)	(e^2b^2)	0.12(14)	0.319(22)*	
Q_s(3/2 ;32.19 keV)	(eb)	-	-0.265(78)*	
B(E2;3/2 →1/2;167.45 keV)	(e^2b^2)	-	≈0.0[b]	

[a] Fit to this c gave χ^2 = 18/DF.

[b] In cases where this parameter was allowed to vary, the result was always consistent with zero.

[c] Average of optical hfs measurements[39] which include Sternheimer corrections[40].

* Statistical error only.

TABLE 7

Line Widths of L and K Transition in ^{202}Hg

Transition	Γ(Hg) - Γ(Pb) (keV)	
	$^2p_{3/2}$	$^2p_{1/2}$
L	-0.13(56)	2.18(75)
K DE	-0.38(45)	3.0 (1.1)
K SE	-0.90(53)	2.4 (1.1)
K FE	-0.02(38)	0.90(75)
MEAN	-0.30(23)	1.90(44)

TABLE 8

$4f_{7/2} - 1s_{1/2}$ Energies

All units are keV. Errors are statistical.

	Experimental $4f_{7/2} - 1s_{1/2}$ Energy	Nuclear[b] Polarization Correction	Vacuum Polarization Correction	Reduced Mass Correction	Corrected $4f_{7/2} - 1s_{1/2}$ Energy
198	9130.62(13)	0.00	0.00	0.00	9130.62(13)
199	9129.11(18)	0.05	0.01	-0.03	9129.14(18)
200	9121.86(15)[a] 9122.48(22)	0.01	0.10	-0.05	9121.92(15) 9122.54(22)
201	9118.02(25)	0.10(20)*	0.13	-0.08	9118.17(32)
202	9111.87(10)	0.19	0.20	-0.10	9112.16(10)
204	9102.44(15)	0.36	0.30	-0.15	9102.95(15)

[a]The two values are inconsistent. See text, Section 5.2.

[b]Error due to change in nuclear polarization is 0.012 keV/neutron.

*See text, Section 5.6.

TABLE 9

Relative Isotope Shifts
Normalized to $\frac{198 - 204}{3} \equiv 1.000$ (arbitrary units)

Pair	μ^-	Optical[b]
198 - 199	0.160(24)	0.1276(12)
198 - 200	0.943(26)[a] 0.876(29)	0.9415(9)
200 - 201	0.407(35)[a] 0.474(45)	0.3143(14)
200 - 202	1.058(22)[a] 1.125(29)	1.0377(9)
202 - 204	0.999(22)	1.0209(26)

[a] Upper value corresponds to $2p_{2/3}$ pathway, lower to $2p_{1/2}$ pathway. See text, Section 5.6.

[b] Reference (14).

TABLE 10

δR_k [a] for muonic x-rays[b], atomic k x-rays[c], and optical transitions[d] for each pair of isotopes. The units are 10^{-3} fm.

	199	200	201	202	204
	1.97(29)	11.55(27)	16.53(47)	24.51(28)	36.75(37)*
198	3.3 (1.5)	12.7 (3.2)	14.2 (2.0)	24.4 (3.0)	36.6 (3.5)
	1.8 (2)	13.2 (1.5)	17.7 (2.0)	27.7 (3.1)	42.1 (4.7)
		9.59(32)*	14.57(49)	22.55(31)	34.78(37)
199		9.4 (2.8)	10.9 (1.6)	21.1 (2.7)	33.2 (3.1)
		11 (1)	15.8 (1.7)	25.9 (2.8)	40.2 (4.5)
			4.98(46)	12.96(25)	25.19(33)
200			1.5 (2.5)	11.7 (1.0)	23.8 (2.3)
			4.4 (5)	14.5 (1.6)	28.8 (3.2)
				7.98(45)*	20.21(49)
201				10.2 (2.3)	22.3 (2.8)
				10 (1)	24.4 (2.7)
					12.23(27)
202					12.2 (3.4)
					14.3 (1.6)

[a] For μ^-, k = 2.413, $C_z = -1.328 \times 10^{-3} \frac{\text{fm}}{\text{keV}}$, for e^-, k = 2.917, $C_z = -78.1 \times 10^{-6} \frac{\text{fm}}{\text{meV}}$.

[b] Includes 0.012 $\frac{\text{keV}}{\text{neutron}}$ uncertainty due to nuclear polarization corrections.

[c] Reference (15)

[d] Reference (14)

* These measurements are free from any geometry dependent energy shift.